



Detection of land degradation risk in Azerbaijan by combining fractional cover estimates based on DESIS data with multi-decadal Landsat NDVI trends

Sarah Asam, Frederic Schwarzenbacher, David Marshall Ingram & Martin Bachmann

To cite this article: Sarah Asam, Frederic Schwarzenbacher, David Marshall Ingram & Martin Bachmann (01 Aug 2025): Detection of land degradation risk in Azerbaijan by combining fractional cover estimates based on DESIS data with multi-decadal Landsat NDVI trends, International Journal of Remote Sensing, DOI: [10.1080/01431161.2025.2536884](https://doi.org/10.1080/01431161.2025.2536884)

To link to this article: <https://doi.org/10.1080/01431161.2025.2536884>



© 2025 The Author(s). Published by Informa UK Limited, trading as Taylor & Francis Group.



Published online: 01 Aug 2025.



[Submit your article to this journal](#)



Article views: 33







[View related articles](#)



[View Crossmark data](#)

Detection of land degradation risk in Azerbaijan by combining fractional cover estimates based on DESIS data with multi-decadal Landsat NDVI trends

Sarah Asam ^a, Frederic Schwarzenbacher ^b, David Marshall Ingram ^a
and Martin Bachmann ^a

^aGerman Remote Sensing Data Center, German Aerospace Center, Wessling, Germany; ^bTopodat – Koenig, Schwarzenbacher & Will GbR, Ulm, Germany

ABSTRACT

Land degradation is a significant environmental issue, exacerbated by climate change and land use pressures. Mountain grassland ecosystems, especially in arid regions, are particularly vulnerable to degradation, leading to reduced vegetation density, biomass and biodiversity, and contributing to soil erosion. While traditional monitoring methods are costly and time-consuming, remote sensing using multispectral data offers a more efficient way to assess large areas continuously. A key challenge in monitoring land degradation, however, is distinguishing between different vegetation cover fractions (fCover) of photoactive vegetation (PV), non-photoactive vegetation (NPV) and bare soil (BS). Hyperspectral data provide better spectral resolution to address this challenge by identifying diagnostic absorption features, but their availability is limited. This study investigates the potential of combining multispectral Landsat and hyperspectral DLR Earth Sensing Imaging Spectrometer (DESIS) data for mapping land degradation risk in Azerbaijan at 30 m spatial resolution. PV was derived for 18 DESIS scenes with a mean average error of 7.1%. Regarding the multi-decadal NDVI time series, 3.8% and 4.9% of the herbaceous vegetated area showed significant negative trends in June and August, respectively. By scaling the BS fCover, negative NDVI trend coefficients and slope steepness maps to a risk score, a degradation risk map for the central-western part of Azerbaijan was generated. Areas prone to degradation were mapped mainly on south-exposed slopes. This approach has high potential for identifying areas recently prone to degradation, facilitating early interventions to prevent the loss of valuable topsoil.

ARTICLE HISTORY


Received 20 December 2024
Accepted 13 July 2025

KEYWORDS

Fractional vegetation cover; VCF; hyperspectral; time series; remote sensing; earth observation; Caucasus

1. Introduction

Degradation is one of the most pressing global environmental issues and is projected to worsen due to climate change and land use pressure (Karlen et al. 2003; Olsson et al. 2019).

CONTACT Sarah Asam  sarah.asam@dlr.de  German Remote Sensing Data Center, German Aerospace Center (DLR), Münchener Straße 20, 82234 Weßling, Germany

© 2025 The Author(s). Published by Informa UK Limited, trading as Taylor & Francis Group.

This is an Open Access article distributed under the terms of the Creative Commons Attribution License (<http://creativecommons.org/licenses/by/4.0/>), which permits unrestricted use, distribution, and reproduction in any medium, provided the original work is properly cited. The terms on which this article has been published allow the posting of the Accepted Manuscript in a repository by the author(s) or with their consent.

Mountainous grassland ecosystems exposed to excessive grazing pressure, especially in arid regions, are particularly prone to degradation (Conant and Paustian 2002; Lewińska et al. 2020; Milchunas and Lauenroth 1993; Zhao et al. 2024). Overgrazing caused by unadjusted stocking rates is mainly observed in grazed mountain areas in developing countries (Neudert et al. 2012; Wiesmair, Otte, and Waldhardt 2017). Land degradation is a process in which the first vegetation is degraded to a lower ecological level, reflected in the reduction of vegetation density, plant biomass and plant species (Liu et al. 2015). As a consequence, soil degradation follows, which leads to salinization and acidification of soils, as well as to an expansion of exposed soil areas, introducing the risk of soil erosion (Bengtsson et al. 2019; Zhongming et al. 2010). Studies (Conant and Paustian 2002; Conant et al. 2017) have shown that rehabilitation of grasslands can potentially lead to increased soil organic matter and carbon sequestration. The proper monitoring of grasslands and the identification, protection and restoration of degraded pastures are hence relevant not only for agriculture productivity and erosion risk but also for ecosystem services such as the functioning of soils as carbon sinks (Conant and Paustian 2002; Neudert et al. 2012).

Monitoring land degradation is usually at the stage of ground investigations, which are costly, time-consuming, and often subjective (White et al. 2000). This restricts the regular assessment of large areas, especially in remote and inaccessible regions (Pi et al. 2021). Conversely, spatially exhaustive and continuous monitoring of vegetation coverage and ecosystem conditions is possible using remote sensing observations (Akiyama and Kawamura 2007; Ali et al. 2016; Dubovyk 2017; M. Reeves et al. 2015; Symeonakis 2022).

Land degradation is mainly assessed in remote sensing by quantifying changes in vegetation indices (VIs) (see e.g. Bai et al. 2008; Le, Tamene, and Vlek 2012; Reeves and Baggett 2014; Wessels et al. 2004) or vegetation parameters such as primary productivity or biomass (see e.g. Fava et al. 2012; Hernández-Clemente et al. 2023; Prince, Becker-Reshef, and Rishmawi 2009; Vlek, Le, and Tamene 2010), which are related to the increase or decrease of vegetation health and/or coverage. Thereby, the multispectral Landsat series of satellites is the most commonly used for land degradation studies based on remote sensing data (D'Acunto, Marinello, and Pezzuolo 2024). Several land degradation indices have been developed that combine different vegetation and environmental indicators derived from remote sensing data (e.g. Guo et al. 2023; Kang, Zhang, and Biswas 2021; Yue et al. 2016), each with specific strengths and limitations in assessing degradation status. Information from long time series is usually needed to detect changes and trends, and frequent observations are needed to distinguish degradation from phenological variability (Dubovyk 2017; Lewińska et al. 2020). For such long-term time series, only multispectral data are currently available. However, multispectral data have limitations in the monitoring of land degradation, as soil reflectance affects VIs, and only green, i.e. photoactive vegetation (PV) can be reliably detected (Abdolzadeh et al. 2020; Asner 1998; Lyu et al. 2020; Wiesmair et al. 2016). Non-photoactive vegetation (NPV), however, is usually confounded with bare soil (BS) because both land covers have similar and featureless spectral reflectance curves in visible (VIS) and near-infrared (NIR) wavelength regions (Nagler, Daughtry, and Goward 2000; Li and Guo 2016). In the context of monitoring land degradation processes, this is problematic, as NPV is, on the one hand, an important component of vegetation productivity in certain grasslands (Asner 1998) and, on the other hand, can significantly reduce the potential for soil erosion compared to BS areas (Arsenault and Bonn 2005; Gyssels et al. 2005; Malec et al. 2015). Especially in regions

where vegetation is sparse and various natural gradients exist, information on the fractions of ground cover (fCover) of PV, NPV and BS is hence important to assess land degradation (Zhang et al. 2013).

Guerschman et al. (2015) provide an overview on studies mapping NPV, PV and BS fCover using multispectral data. A current state-of-the-art as well as an evaluation of the derivation of long-term trends in fCover based on Landsat data through a Multiple Endmember Spectral Mixture Analysis (MESMA) approach is given in Lewińska et al. (2025). Hyperspectral data, however, are particularly valuable in this regard as they have the spectral resolution required to distinguish soil, vital and dry/dormant vegetation (Cooper et al. 2020; Gamon, Peñuelas, and Field 1992; Li and Guo 2016; Obermeier et al. 2019). Since the 1990's, hyperspectral data have been the focus of research regarding this issue (see references in Bachmann 2007). The fundamental developments were made using airborne hyperspectral data covering the entire spectral range from VIS to short-wave infrared (SWIR) wavelength regions and included the development of various MESMA approaches such as in Roberts et al. (1998), Asner and Lobell (2000), García-Haro, Sommer, and Kemper (2005) or Bachmann (2007). The basis of these approaches is the concept that the spectral variation of surfaces is due to the contribution of various mixtures of materials which have their own spectral reflectance.

Still, the availability of hyperspectral data is a limitation for consistent, continuous and area-wide mapping of fCover. Ongoing research is mostly limited to experimental methods based on simulated hyperspectral data (Liu et al. 2014) and on hyperspectral data collected using unmanned aerial vehicles (UAVs) over small regions. For example, Pi et al. (2021) used airborne hyperspectral UAV data to classify species groups for indicating grassland degradation. Only a few studies exist employing larger-scale hyperspectral data from sensors mounted on airplanes or satellites. Lyu et al. (2020) introduced an approach for grassland degradation monitoring, which is based on the spectral unmixing of Hyperion data for species composition monitoring in an area of Inner Mongolia, China. Wang et al. (2020) also mapped species by simulating hyperspectral reflectance based on multispectral HJ-1A images. Zhang et al. (2013) used hyperspectral HJ-1 data to map fCover over a study area in China using the dimidiate pixel decomposition model. In order to use vegetation cover information to further assess soil erosion, Malec et al. (2015) employed simulated EnMAP data to derive fCover estimates with the MESMA approach. The fractions for PV, NPV and BS were then integrated into a formula to calculate the C-factor (cover management parameter) for the Revised Universal Soil Loss Equation (RUSLE). Also, Bracken et al. (2019) tried to detect soil erosion directly from simulated EnMAP data in a Mediterranean area. They calculated fCover through the MESMA approach and used the fractions to mask out vegetated areas in the raw data.

This overview on studies assessing land degradation using hyperspectral data shows that while the techniques are already quite developed, the research community is mainly limited to small scale and mono-temporal analysis. This also includes the scarce use of data from the hyperspectral DLR Earth Sensing Imaging Spectrometer (DEGIS) sensor for vegetation monitoring. So far, only a handful of studies investigate the capability of DEGIS data for mapping of biodiversity or species (Gholizadeh et al. 2022; Kamaraj et al. 2024; Mafanya et al. 2022; Pacheco-Labrador et al. 2021, 2022), vegetation traits or productivity (Campbell et al. 2021; Huemrich et al. 2021) or crop-type classification (Aneece

and Thenkabail [2021](#); Aneece et al. [2022](#)). Area-covering mapping is rarely demonstrated using any hyperspectral sensor, and the temporal variability of vegetation in semi-arid areas has also not been considered.

As one aspect of this study, we therefore aim to investigate the potential of hyperspectral data for large-scale environmental monitoring in Azerbaijan. In the Caucasus region, livestock farming is an important part of the agricultural sector, and subsistence farming is commonplace; hence, threats to pastures can significantly impact livelihoods (Neudert et al. [2012](#)). As in other post-Soviet transition countries (Akhmadov, Breckle, and Breckle [2006](#); Borchardt et al. [2011](#)), overgrazing has become relevant in the Caucasus in recent decades. Furthermore, grazing impact increased in many places due to the replacement of sheep husbandry with localized cattle farming (Wiesmair et al. [2016](#)). Accordingly, livestock numbers in Azerbaijan are growing (The State Statistical Committee of the Republic of Azerbaijan [2023a](#)), and Azeri grassland areas are under heavy grazing pressure, leading to vegetation cover loss and erosion (de Leeuw et al. [2019](#); Neudert et al. [2012](#)). However, despite the relevance of grassland ecosystem functioning in this region and the need for timely, spatially exhaustive and cost-effective monitoring, remote sensing-based research on grassland conditions in the Caucasus region is still limited (see e.g. Buchner et al. [2020](#); de Leeuw et al. [2019](#); Lewińska et al. [2020](#); Magiera et al. [2013](#); Wiesmair et al. [2016](#)).

The aim of this study is therefore to fill this gap and to assess the potential of combining multispectral time series with mono-temporal hyperspectral data for large-scale grassland monitoring. Based on the combined use of fCover estimates derived from 18 DESIS scenes and a country-wide multidecadal time-series analysis of Landsat-based Normalized Difference Vegetation Index (NDVI), we aim to answer the following questions in this study:

- Can DESIS data be used for the retrieval of cover fractions of PV, NPV and BS using linear spectral unmixing?
- Does the combined use of long-term NDVI trends and mono-temporal fCover estimates result in reasonable patterns of current land degradation risk?

The underlying hypothesis of this study is that NDVI and fCover represent different vegetation traits, and that combining long-term NDVI trends with recent fCover estimates can improve the identification of vegetated areas prone to degradation. In particular, NPV and BS information are critical for mapping degradation, as BS is at higher erosion risk than NPV-covered soils, yet multispectral data generally struggle to distinguish between these two cover fractions. Although the DESIS data used in this study – from which NPV and BS information can be derived – provide only mono-temporal information, the NDVI trend spans several decades. By using BS fractions, negative NDVI trends and slope steepness as factors in a risk score, we aim to enhance multi-decadal assessment of vegetation change by incorporating canopy structure information from hyperspectral DESIS data. To our knowledge, no previous study has combined multi-decadal NDVI trends with fCover estimates derived from hyperspectral data to assess land degradation risk (D'Acunto, Marinello, and Pezzuolo [2024](#)).

2. Materials and methods

2.1. Study area

The study area is the Republic of Azerbaijan located in the South Caucasus region (see [Figure 1](#)). Azerbaijan has an extent of 86,600 km² and a varied topography, characterized by the mountain regions of the Greater and Lesser Caucasus (covering 40% of the country) and extensive lowlands, the so-called Kura-Aras basin, in central-southern parts of the country. Annual precipitation varies between up to 1800 mm at the South-East Caspian Sea coast, above 600 mm in the mountain regions, lower values in the Kura-Aras basin and driest conditions in the Eastern lowlands of Absheron, with precipitation sums ranging from 200 to 350 mm. Temperatures could reach maximum values of up to 45°C and minimum values down to −33°C.

About one-third of the country is covered by grasslands, with an extent of approx. 25000 km² (The State Statistical Committee of the Republic of Azerbaijan [2023b](#)), which is about half of the utilized agricultural area (The State Statistical Committee of the Republic of Azerbaijan [2023c](#)). Transhumant livestock keeping is the major production system, which coexists with mostly small-scale sedentary livestock farms. Depending on altitude and condition, grasslands are used seasonally as winter and summer pastures. Every year, several million animals migrate between the summer pastures in the mountains and the winter pastures in the semi-arid lowlands. Summer pastures are covered by different kinds

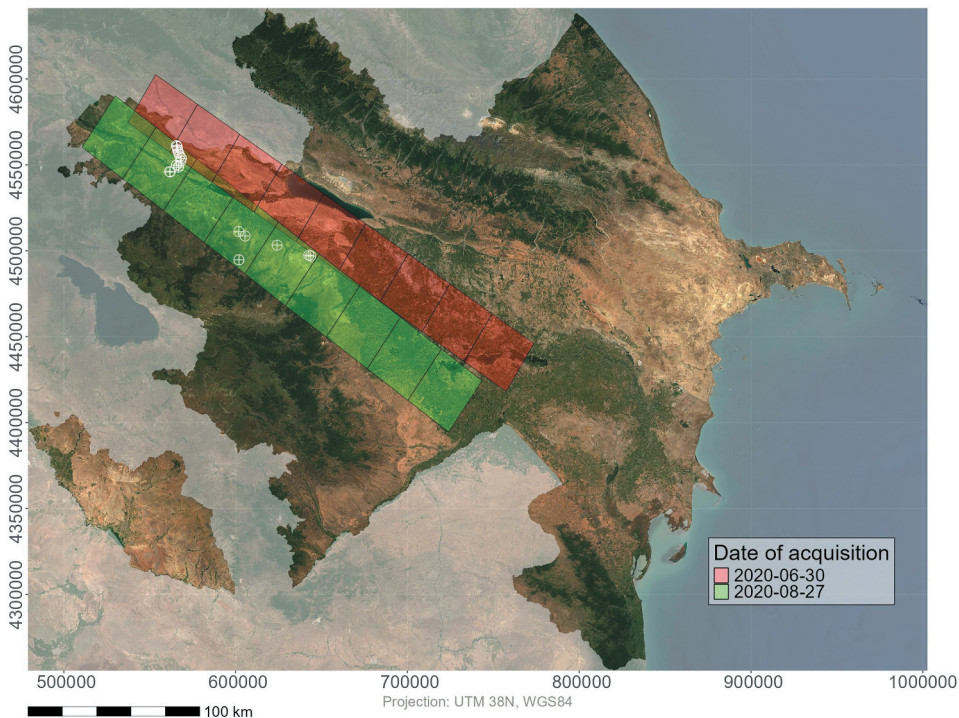


Figure 1. Extent of the study area of Azerbaijan with the DESIS tile footprints and the location of the in-situ sampling plots displayed in white (background map contains modified Copernicus Sentinel data 2022 (EOX IT Services GmbH [2022](#))).

of grasslands, which are similar to central European such as *Nardus*-dominated grasslands. The winter pastures are mainly used from November until March. Grasslands in direct periphery of villages and townships are used as common pastures during the whole year.

The grassland areas of Azerbaijan are under heavy anthropogenic pressure from unsustainable management practices, land use conversion and climate change. Due to missing responsibilities and inadequate management, the grazing intensity often exceeds the carrying capacity of grasslands (de Leeuw et al. 2019). The winter pastures, which are located in drier and hotter lowlands, are not productive but under high grazing pressure. In the Greater Caucasus, on the other hand, erosion is a common risk due to overgrazing, deforestation and specific soil conditions. The humus layer and A-Horizon are usually very thin, and through trampling by cattle, cracks and fissures can develop in the upper soil layer. In the case of heavy rainfall, water can inundate into these cracks and saturated soils at some point slide off. Therefore, large-scale landslides are quite common in this region, affecting mainly summer pastures (Köstl, Wuttej, and Kirchmeir 2018). However, the common pastures as well as the main migration routes between summer and winter pastures are under high pressure, too (Iniguez et al. 2005; Wiesmair et al. 2016). The most heavily eroded areas are often adjacent to human settlements. In contrast, more sustainable land use including practices such as rotation system, mowing and bee keeping can be found on former kolkhozes (Köstl, Wuttej, and Kirchmeir 2018).

2.2. Data

2.2.1. DESIS

The DESIS instrument is an imaging spectrometer installed on the Multi-User-System for Earth Sensing (MUSES) platform on the International Space Station (ISS) since September 2018. It features 235 spectral channels ranging from 400 nm to 1000 nm, covering the VNIR region with a spectral sampling distance of 2.55 nm and a Full Width Half Maximum (FWHM) of about 3.5 nm (see Figure 2). The spatial resolution of the DESIS imagery is 30 m (Alonso et al. 2019; Carmona et al. 2022; Krutz et al. 2019).

Eighteen DESIS acquisition tiles recorded in June and August 2020 over Azerbaijan were selected, forming transects through the Kura-Aras basin and Lesser Caucasus in the western part of Azerbaijan and covering about one-fifth of the country area (see Figure 1). Imagery filtering criteria were a cloud coverage of <25% and a sun zenith angle of <40°. For the derivation of the fCover components, several pre-processing steps were carried out. The DESIS processing chain includes the radiometric and spectral calibration as well as the correction of further sensor effects like rolling shutter and spectral smile (Alonso et al. 2019). The L2A data were ortho-rectified as well as atmospherically corrected, providing additional cloud and haze masks. In this study, the first nine bands (wavelength 402–442.5 nm) were excluded from further analysis, due to possible artefacts in these bands originating from the detector manufacturing (Carmona et al. 2022), as well as all bands above 883 nm influenced by etaloning (see Figure 2). The exclusion of these wavelength ranges does usually not affect the quality of the fCover analysis, as shown in previous studies (Bachmann 2007). For a trade-off between the required spectral resolution and the signal-to-noise, a 2x binning was applied, leading to a ~10 nm bandwidth per channel. The DESIS L2A data include quality masks, which were used to

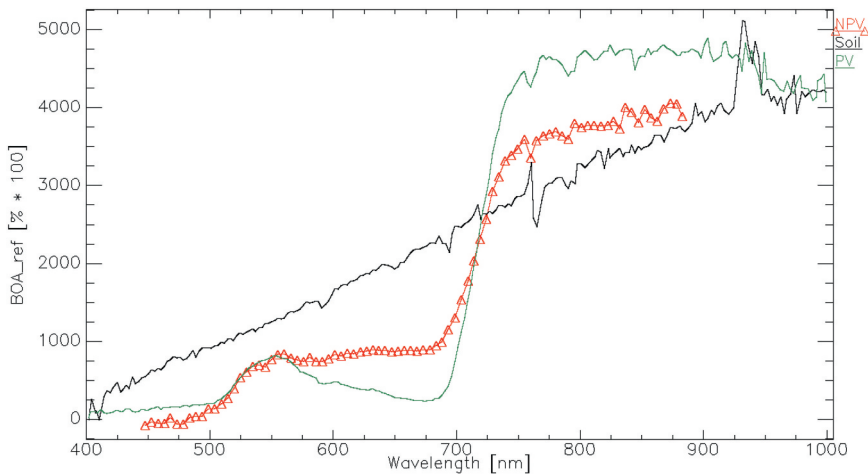


Figure 2. Typical DESIS L2A spectra at full spectral resolution (235 bands) for PV (green) and soil (black), and for NPV as processed for usage in this study (in red, triangles represent band centres; processing is 2x binning, spectral subset of 447 nm to 883 nm). Note that DESIS L2A processing can result in slightly negative reflectances, on purpose, ensuring a proper spectral shape even when Aerosol Optical Thickness (AOT) retrieval is slightly off.

further mask out pixels covered by cloud shadow, clouds and snow. Finally, a land cover mask (see section 2.2.4) was applied to limit the DESIS spectral data to herbaceously vegetated and bare soil areas, i.e. excluding forests, shrubland, water and artificial surfaces, which is an essential step for the further endmember (EM) identification and classification in the fCover processor (see section 2.3.1).

2.2.2. Landsat time series

In June and August, NDVI time series (1987–2021) were created to detect grassland condition trajectories in Azerbaijan based on multi-decadal vegetation condition observations from the NASA Landsat Missions (TM, ETM+, OLI) at 30 m spatial resolution (Masek et al. 2006). Data processing was conducted on the Google Earth Engine (GEE) platform (Gorelick et al. 2017), where the acquisitions were filtered to a maximum cloud cover of 90%. All used Landsat data were scaled with the officially provided parameters (USGS 2021, 2022) to transform the pixel values from digital numbers to reflectance values. In a further step, TM & ETM+ sensor data were harmonized to the OLI data as suggested by Roy et al. (2016) and in the GEE guidelines (Braaten 2024). Clouds and cloud shadows were masked out using the mask layers created with the fmask processor (Zhu, Wang, and Woodcock 2015). The images were then limited to grassland, cropland and barren/sparse vegetation pixels using a land cover mask (see Section 2.2.4). Pixelwise June and August NDVI of these areas for each year are generated through calculating the respective monthly median NDVI based on all available scenes. This procedure was chosen in order to generate consistent time series for which the influence of outliers, e.g. due to undetected clouds, is minimized (Asam et al. 2023). Median NDVI maps for June and August of all years are calculated to fit the phenological stages captured in the DESIS data (see Section 2.2.1).

To avoid gaps in the monthly median NDVI composites, a tolerance timespan was defined to fill missing pixels, e.g. resulting from clouds, as follows: for the June time-series, the tolerance timespan is from beginning of May until mid of July. For the August time-series, the tolerance timespan ranges from mid-July until the end of September. For each missing pixel, the closest valid observation in time from the 15th of the corresponding month was searched in the tolerance timespan. No further pre-processing such as filtering or smoothing was applied.

2.2.3. In-situ data

In-situ data have been collected in Azerbaijan in order to retrieve information on the fractional vegetation cover and erosion risk in the study area. The distribution of the plots was designed to cover all varieties of pastures and meadows that can be found in Azerbaijan with regard to exposition, elevation, species composition and management. In total, information was collected at 296 sample plots in the western, northern and southern parts of the country by the E.C.O. Institute of Ecology (E.C.O. Institut für Ökologie Jungmeier GmbH 2023) during two field campaigns in August and October 2018. The only region that had to be excluded was the politically unstable region of Yukhari-Garabakh in the southwest of the country. At each 30 × 30 m plot, general information such as elevation, inclination, exposition, management and predominant vegetation type was recorded. In addition, the overall vegetation ground coverage in percent regarding only living biomass, the potential maximum vegetation coverage and the erosion intensity in five categories (none – very high) were estimated. Besides these attributes, every plot was documented photographically. Five pictures have been taken from the centre of the site, covering all directions and one looking vertically downwards. The in-situ sampling was restricted to grassland areas as well as to some phenologically very similar classes for which a high confusion risk was anticipated (such as bushland, shrubland, semi-desert-vegetation and cropland) (Köstl, Wuttej, and Kirchmeir 2018). After intersection with the DESIS acquisition footprints, land cover masking, cloud masking and filtering for vegetation type recorded in the field, 27 sampling points remained for validation (see Figure 1).

2.2.4. Land cover mask

The ESA WorldCover land cover classification v100 (Zanaga et al. 2021) at 10 m spatial resolution was used in this study. The classification is based on Copernicus Sentinel-1 and Sentinel-2 data referring to the year 2020 and distinguishes 11 classes. It reaches an overall accuracy of 74.4% (Tsendbazar et al. 2021). The land cover classification was resampled to 30 metres in order to meet the spatial resolution of the DESIS and Landsat data and reprojected to UTM projection. The classes 'grassland', 'cropland' and 'barren/sparse vegetation' were aggregated as the mask area, and the resulting binary map was majority sieved using a threshold of 10 pixels in order to reduce noise in the land cover mask. The classes 'cropland' and 'barren/sparse vegetation' were included in order to catch also very densely as well as very sparsely vegetated areas for the EM generation.

2.2.5. Topography

Void filled topographic data from the Shuttle Radar Topography Mission (SRTM) at a resolution of 1 arc-second (SRTMGL1 version 3 by NASA JPL; Farr et al. 2007) were

derived via the GEE platform (Gorelick et al. 2017) and projected to match the UTM coordinate system of the above mentioned data. The topographic dataset is used to conduct analyses of the NDVI trend and the fCover related to topographic variables, such as elevation and slope, and for the land degradation risk analysis.

2.3. Methods

The concept followed in this approach is to derive a degradation risk map based on a degradation risk score, which is calculated by scaling the BS fCover, negative NDVI trend coefficients and slope steepness. After describing the generation of the required datasets, i.e. fCover based on DESIS data (Chapter 2.3.1) and NDVI trends (Chapter 2.3.2), the calculation of the degradation risk map is detailed in Chapter 2.3.3.

2.3.1. fCover derivation

fCover derivation is based on the spectral unmixing of hyperspectral DESIS data. Especially in dryland areas with a heterogeneous and patchy distribution of vegetation and soils, the sensed signal within a pixel almost always consists of a mixture of different cover types. The inversion process of spectral unmixing allows for the retrieval of different material fractions within a pixel and thus an approximate subpixel quantification of vegetation and soil cover fractions.

For each DESIS scene, fCover was calculated using the ‘fCover’ processor developed at DLR (see Figure 3) (Marshall et al. 2021). In order to account for the spectral variability of the different materials in a scene, MESMA approaches were developed (Asner and Lobell 2000; Bachmann 2007; García-Haro, Sommer, and Kemper 2005; Roberts et al. 1998) where the material spectra are grouped into thematic classes such as PV, NPV and BS. The combination

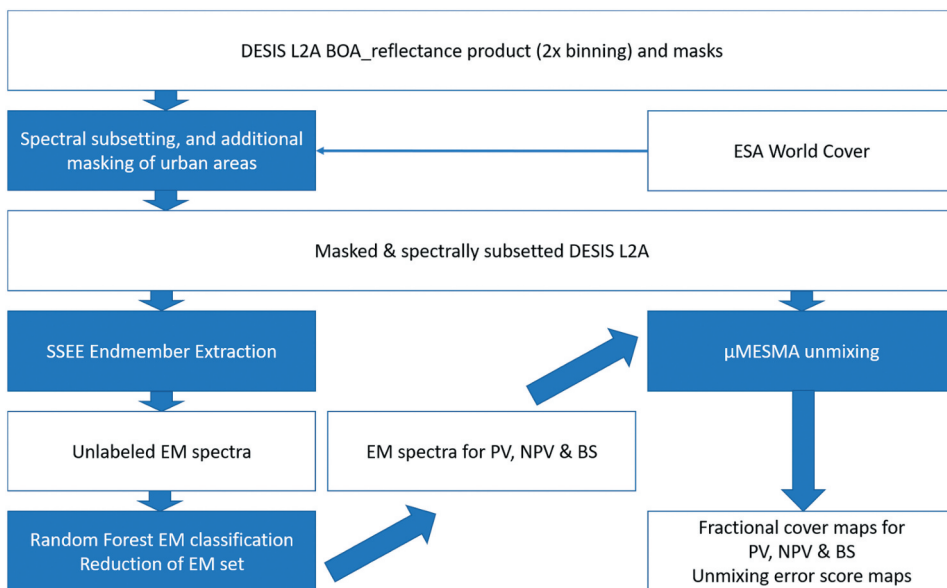


Figure 3. Workflow of the fCover estimation approach.

of one spectrum of each class is simultaneously used for unmixing a pixel, calculating all existing combinations. One prerequisite for MESMA is that the spectra of the pure materials (denoted as EMs) are derived beforehand, which is commonly conducted by an estimation of the extremes in a transformed feature space, followed by a labelling process. We conducted the estimation of spectrally extreme pixels, i.e. pure material signatures, by the Spatial-Spectral Endmember Extraction (SSEE) (Rogge et al. 2012; Rogge et al. 2007) using the original implementation. The labelling of the classes PV, NPV and BS is achieved by a random forest classifier ($n_estimators = 1865$, $min_samples_split = 6$, $min_samples_leaf = 3$ and $max_features = \text{square root}$) trained on an extensive library of field spectra (see Paulik 2018 and Ziel et al. 2019 for details). For the reduction of the EM libraries, thresholds for the metrics proposed by Dennison and Roberts (2003) were used (i.e. Class-Average RMSE (CAR) and EM average RMSE (EAR)), resulting in a set of pure and representative EM spectra for each labelled class. Additionally, an EM for 'shade' is included in the unmixing, accounting for illumination and overall brightness effects. In the unmixing process, the fraction of this shade class can indicate brightness effects, missing EMs in the spectral library or an inadequate masking of the input files, respectively. The linear mixture model can therefore be written as

$$\rho_{\text{Sensed}} = f_{\text{PV}} \times \rho_{\text{PV}} + f_{\text{NPV}} \times \rho_{\text{NPV}} + f_{\text{BS}} \times \rho_{\text{BS}} + f_{\text{Shade}} \times \rho_{\text{Shade}} + \varepsilon \quad (1)$$

with ρ_{Sensed} being the ground reflectance of an image pixel, ρ denoting the EM signature for PV/NPV/BS/Shade, f the fractional cover of the respective EM and ε the residual error. The ground cover fractions for each pixel can then be estimated by inversion of the linear mixing model. f Covers are hence calculated using μ MESMA (Bachmann, Muller, and Dech 2009) with each pixel treated as a linear combination of each spectral class, where the residual error term is minimized given the constraints that individual fractions are within [0 - 100%] and that the sum of fractions is equal to 100%. Within most MESMA approaches, the final EM and related unmixing model are selected by the lowest residual represented by the modelling RMSE (ε). For μ MESMA used in this study, the final model selection criteria are a combined unmixing model score with a band weighting of the modelling RMSE and a penalty score for unrealistic abundances (e.g. negative or above 100%) as well as penalty for violation of the sum-to-one criterion as an unconstrained solver (pseudo-inverse) (see Bachmann 2007 for details). Following the approach of Garcia and Ustin (2001), the influence of the shade component is removed in a final step through rescaling the abundances for PV, NPV and BS. In order to avoid numerical issues, negative abundances are set to a small positive value of 0.001 for this procedure. More information on the workflow and its application is given in Malec et al. (2015) for soil erosion in Costa Rica, Bayer et al. (2016) in the context of the retrieval of soil parameters in South Africa, and Bachmann (2007) for land degradation in Spain and providing the full unmixing methodology.

The available in-situ data include information on living vegetation coverage in percent at the time of the data sampling as well as estimates on the yearly maximum vegetation coverage (see section 2.2.2). The current living vegetation coverage from the field was used to create evaluation metrics for the PV fraction. At each in-situ point, the abundance fraction of PV was extracted from the unmixing results and subtracted from the field information. The mean of all absolute abundance difference values was calculated and is presented as the mean absolute error (MAE). Additionally, the standard deviation (SD)

between all absolute difference values is provided. Scatter plots are created to assess variance and bias in the PV estimation. A vertical error bar shows the Root Mean Square Error (RSME) of the unmixing for the corresponding pixel. Additionally, the seasonal shift between the in-situ sampling and the DESIS acquisition is displayed in a number of days next to each scatter point. The plot also includes colour coded information on the landscape heterogeneity of the sampling site, which is roughly estimated by interpreting the available photos from the corresponding sites.

2.3.2. Time series analysis

From the monthly median NDVI maps for June and August 1987–2021 (section 2.2.2), trends of the NDVI were derived. Only positive NDVI values were included in the trend analysis, as negative NDVI is assumed to represent neither vegetation nor soil (such values e.g. occur sporadically at the shores of reservoirs with varying water levels) and can severely affect the trend detection. The Sen's slope (Sen 1968) and the Mann-Kendall test (Kendall 1975; Mann 1945) were used for trend detection. The Sen's slope was calculated by using a temporal interval of '1' for each time stamp (year). Trends are considered significant if they have p-values lower than 0.05, which is a common threshold representing a statistical significance at the 95% level where non-significant trends are masked out. Additional outputs of the processing are the monthly sums of valid pixels that were included in the calculation of the median, as well as the sum of available monthly NDVI pixels over the whole time series, both for the monthly and the extended compositing periods.

2.3.3. Vegetation pattern and degradation risk assessment

To assess vegetation patterns and gradients in Azerbaijan from field- to landscape scale, as well as to detect artefacts and assess the plausibility of the resulting maps, fCover estimates are first analysed for each season by visualizing their spatial patterns. Accordingly, the June and August NDVI trend datasets are examined for significant positive and negative trends both on a country-wide scale and within the areas covered by DESIS acquisitions. A rough classification based on elevation (>1600 m a.s.l. for sub-alpine, <800 m a.s.l. for lowland) allows for a comparison of processes in the summer and winter pastures (de Leeuw et al. 2019; Neudert et al. 2012). The effect of the exposition is analysed by correlating NDVI trends with slope and aspect using Spearman's rank correlation (Neudert et al. 2012). For consistency analysis, the DESIS fCover fractions and the long-term NDVI trends for June and August are correlated using Spearman's rank correlation, overlaying both datasets within the DESIS footprints for each season.

The primary objective of this analysis is to assess land degradation risk by combining long-term vegetation changes with detailed estimates of current canopy properties from fCover. Degradation risk is assessed by identifying areas undergoing a decline in vegetation abundance, mapped through NDVI changes over time. Additionally, PV, NPV and BS fCover are mapped to identify areas with sparse or no vegetation cover, and information on NPV coverage, which is not captured by the NDVI signal, is separated from BS shares to refine this analysis. Areas with low NDVI but still significant NPV coverage are assumed to have a lower degradation risk, as the topsoil is better protected than in areas dominated by high BS shares. Hence, the primary focus is on BS estimates, as PV and NPV both act as protective ground coverage against soil erosion. Areas with higher proportions of BS

cover are generally more prone to degradation (Malec et al. 2015; Wiesmair et al. 2016; Wiesmair, Otte, and Waldhardt 2017; Zhongming et al. 2010), particularly when located on steep slopes (Neudert et al. 2012).

Only areas which exhibit all three features – low fractional vegetation cover, a reduced NDVI compared to earlier stages and a location on a slope – are mapped as having an increased risk of degradation. Given that all these factors contribute gradually to degradation risk, we take advantage of the continuous nature of the datasets by scaling them relative to one another, avoiding the introduction of artificial thresholds or categories. The fCover of BS (f_{BS} , scaled from 0 to 1) is hence multiplied with a significantly negative NDVI trend coefficient (S_{NDVI} , scaled from 0 to 1) and topographic data on slope steepness (s , also scaled to 0–1):

$$s_r = f_{BS} \times S_{NDVI} \times s \quad (2)$$

This creates a risk score s_r , indicating locations of increasing degradation risk, which is then analysed in terms of topography and land cover classes.

3. Results

3.1. fCover

Continuous and seamlessly mergeable fCover estimates could be derived for all 18 DESIS tiles. Before scaling, the abundance fractions for PV, NPV and BS show mean values of 12%, 19% and 30%, respectively, in the June scenes, and 15%, 22% and 21%, respectively, in the August scenes. As expected, the scaled cover fractions are consistently higher, with mean PV, NPV and BS coverage values of 20%, 32% and 49%, respectively, in June, and 24%, 39% and 37%, respectively, in August. In the June acquisitions, about 17% of the covered areas are dominated by PV, 23% by NPV, and in 60% of the area, BS has the highest share (both for the unscaled and the scaled cover fractions). This distribution is different in the August scenes covering more lowlands, when about 23% of the areas have the highest shares of PV, 37% are mainly covered by NPV and the remaining 40% are predominantly covered by BS.

For the ecological interpretation of the results, the main landscape patterns are depicted in the DESIS transects (see Figure 4), spatially from rather dry and mountainous conditions in the West, to agriculturally more intensively used pastures and cropland areas in the East along the river Kura, and at the foothills and foreland of the Karabakh Range. The upper figure shows the scaled fCover as mapped at the end of June 2020, while the lower figure shows the situation a bit further to the south, mapped at the end of August 2020. More spatial details are given in the subsets of Figure 4. The white subset in the June image depicts a cold-arid steppe region at the border with Georgia. The ridge in the centre of the subset has vast areas of BS, especially on South exposed slopes, while the North exposed slopes in the South-Western part of the subset show relatively high shares of NPV vegetation. A few patches of high PV shares are scattered in the centre and the lower right corner of the subset, which are presumably agricultural fields irrigated through ditches and circular sprinkler systems, as well as along the river Gabirri in the upper part of the scene. The black subset in the June transect is located at the river Kura around the Rayon capital of Zərdab, which is part of the Arran economic region. The

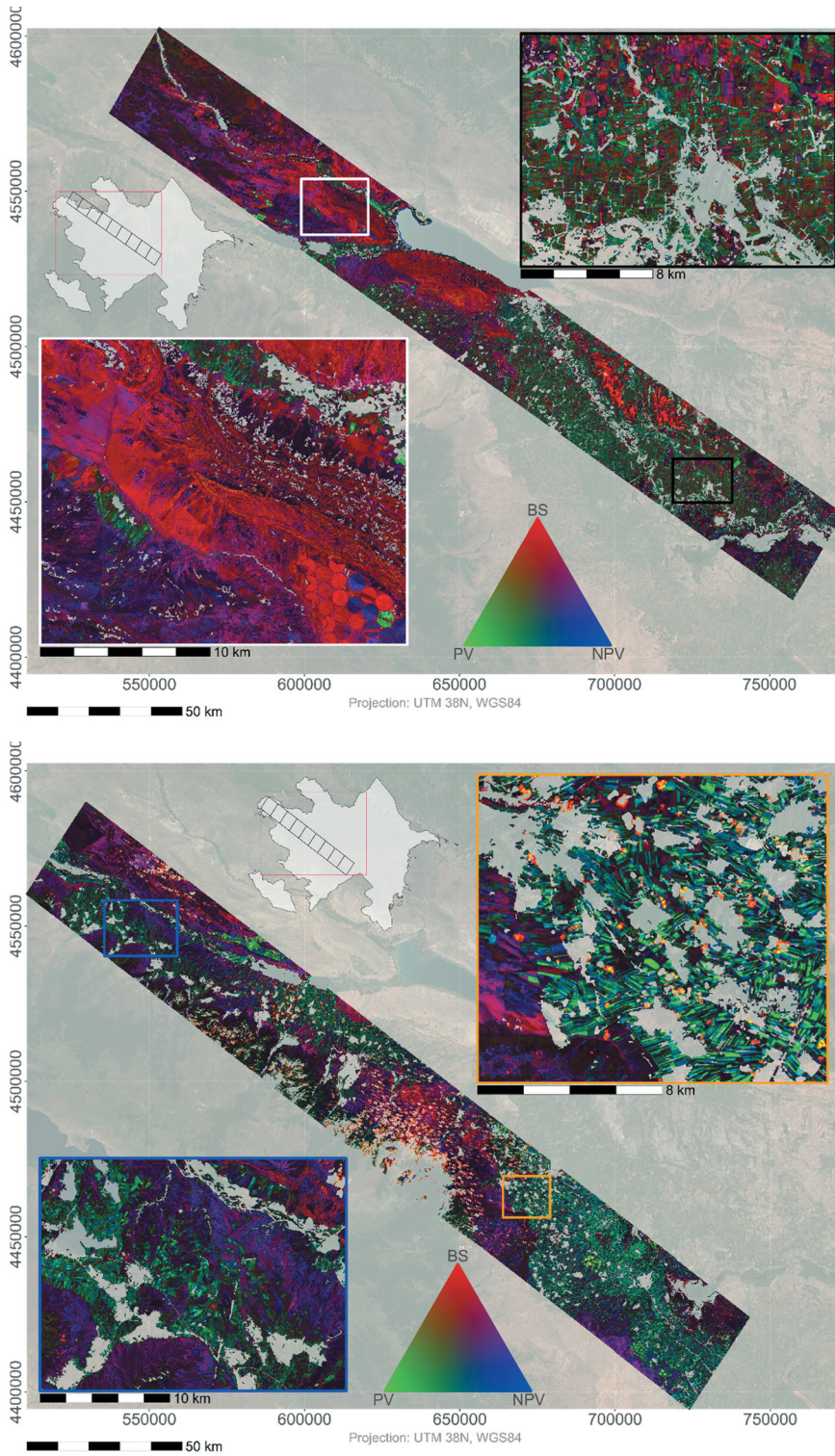


Figure 4. RGB representation of the mosaics of the fCover maps derived for the June (top) and the August acquisitions (bottom). The scaled PV, NPV and BS fractions are displayed in shades of green, blue and red, respectively. The subsets show examples of typical landscape features (see text for further descriptions).

landscape is dominated by its agrarian use in a multitude of small-scale fields, traversed by a network of channels. Most fields, especially those close to rivers, have a high share of PV, while smaller and more remote fields have high shares of BS. These could either be recently mown or harvested parcels, which are being prepared for a second crop. With large parts of the region located around or below the sea level, non-vegetated areas depicted in bright red could also be permanently bare land affected by salinization (Ismayilov et al. 2021). Blue NPV pixels are found predominantly in fields remote from the rivers, which might be fallow or less intensively used, and at the border of parcels. These probably indicate dry or shrub vegetation along field edges and canals.

The August transect differs from the June transect in an overall smaller share of BS fractions, with at the same time a higher fraction of NPV. The north-western subset covers the area between the foothills of the Lesser Caucasus and the Kura river around the town of Ağstafa, at the Armenian border. High fractions of PV intermixed with NPV are located on the agricultural fields, while high NPV fractions can be found on the grassland covered north-facing mountain slopes in the south and centre of the subset. Only on the south-exposed slopes on the opposite shore of the Kura river, larger areas of high BS fractions can be found. Spot-like small areas of BS at the southern edge of the subset can be associated with mining activities. The south-eastern subset close to Tərtər is also characterized by higher shares of NPV, on sloping grasslands as well as on flat agricultural fields. This is in accordance with the growing season and cropping patterns of the region. During the autumn, senescent plant parts such as cotton bushes or cereal litter are often left on the fields to be grazed by livestock.

When comparing the fCover derived from DESIS with the field measurements (Table 1), the MAE for the green vegetation (PV) is 6.70% (SD \pm 5.81%) for the original and 7.05% (SD \pm 5.51%) for the scaled PV estimates (shadow component removed). These MAEs for green vegetation are in the expected range of the method. The Spearman correlation coefficient between the estimated and measured PV is 0.52 (p-value <0.01), and RMSE = 8.8%.

From the scatterplots displayed in Figure 5, it can be seen that the PV estimates from both in-situ and DESIS are generally low, mostly below 20% abundance. The agreement between both estimates is mostly within $\pm 10\%$, but with the tendency that PV is overall slightly underestimated. The scaled PV data cover a more realistic data range and through this have a wider spread, but mostly follow the 1:1 line apart from some outliers. These outliers might be associated with either a large seasonal offset between the day of acquisition and the day of reference data sampling (e.g. 59 days for the sample to the right of Figure 5(a)) or the high spatial heterogeneity of the landscape (e.g. a grassland site with considerable shrub coverage indicated in red towards the top of Figure 5(b)). Taking this time difference and the unmixing RMSE (error bars in Figure 5) into account, the scaling results in a better representation of the data range for PV, despite having a slightly higher overall MAE.

Table 1. Evaluation metrics of PV estimation based on in situ observations.

	MAE	SD of absolute errors
PV	6.70	5.81
PV scaled	7.05	5.51

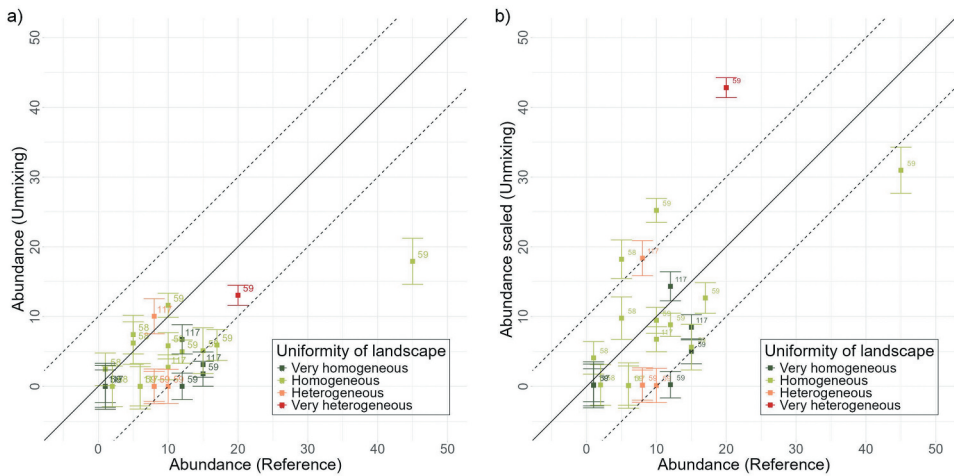


Figure 5. Validation scatter plot of PV (a) and scaled PV (b). The vertical error bars show the RMS score of the spectral unmixing for the respective pixel (scaled by factor 0.01). The number annotations indicate the seasonal shift between DESIS acquisition and reference data in days, and the colours indicate the uniformity of landscape of the respective in-situ plot. Dashed lines indicate a derivation by $\pm 10\%$.

The other cover fractions of NPV and BS could not be validated based on the available in situ observations. However, a correlation analysis between the combined NPV and BS shares and the monthly 2020 median NDVI indicates plausible negative relationships (Spearman $r = -0.64$ and $r = -0.65$ for June and August, respectively). We hence assume also the NPV and BS to be plausible fCover estimates.

3.2. Vegetation condition trend detection

Based on the monthly median NDVI composites for the years 1987–2021, significant NDVI trends for June and August could be derived. The underlying data basis for these calculations was improved through the integration of data from the extended tolerance timespan, resulting in almost one June and August composite each year, when filling the gaps with data from previous/following weeks.

Figures 6 and 7 visualize the significant ($p < 0.05$) NDVI trends in Azerbaijan for 1987–2021 in June and August. In Table 2, the area percentages of positive and negative NDVI trends are summarized for the entire analysed vegetated area (differenced for grassland, cropland and sparsely vegetated areas), only for the area covered by the DESIS acquisitions, as well as for summer and winter pastures. Overall, more areas underwent positive than negative NDVI trends in both seasons. In June, 11.1% of the analysed areas have significant positive NDVI trends, while 3.8% have negative trends. Similarly, in the August NDVI time series, 10.4% of the pixels have positive and 4.9% have negative NDVI trends. Partitioned according to the land cover classes, the analysis shows that 3.0% (3.6%) of Azerbaijan's grasslands, 4.3% (5.6%) of cropland and 5.5% (7.6%) of sparsely vegetated areas show negative trends in June (August). Hence, overall only small shares of the herbaceously vegetated areas undergo a decrease in vegetation conditions. Sparsely vegetated areas are affected the most, followed by cropland, and negative NDVI trends in August are slightly higher compared to June.

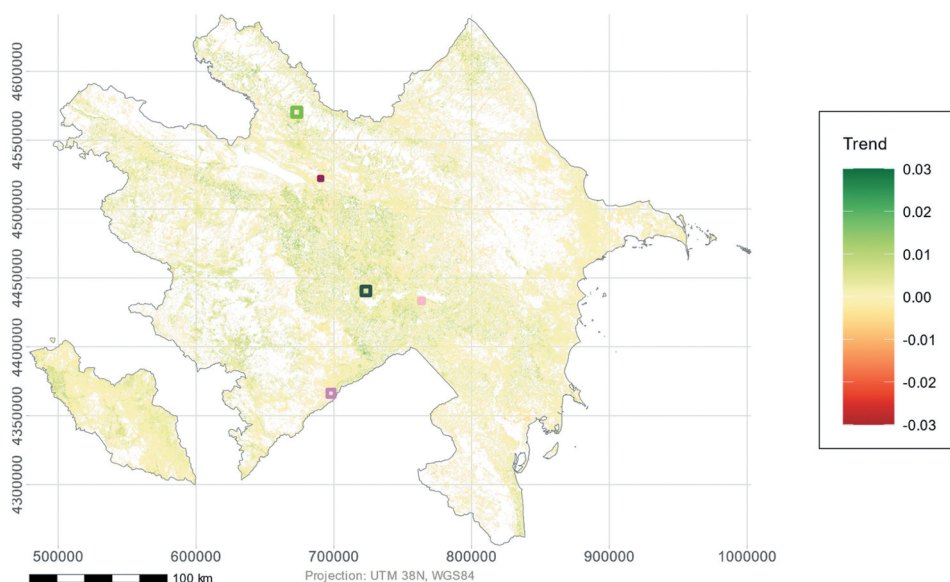


Figure 6. Significant NDVI trends for the years 1987–2021 in June. The colour scale depicts the trend slope value. The coloured boxes refer to the subsets shown in [Figure 9](#).

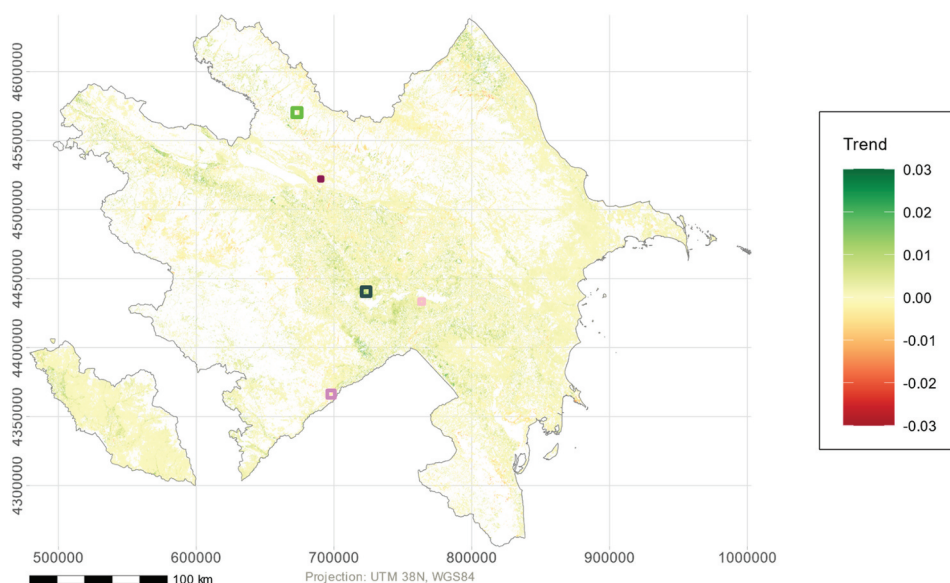


Figure 7. Significant NDVI trends for the years 1987–2021 in August. The colour scale depicts the trend slope value. The coloured boxes refer to the subsets shown in [Figure 9](#).

When looking at the area covered by the DESIS footprint only, the patterns are overall similar ([Table 2](#)), indicating that it represents a large part of landscape types in Azerbaijan. However, in the DESIS focus area, the cropland area stands out, with distinctively higher area shares of positive NDVI trends (16.8% in June and 14.7% in August). This might be caused by the dominance of intensively used agricultural areas in the Kura-Aras basin, on which

Table 2. Area percentage of positive and negative NDVI trends for Azerbaijan on a country-wide scale, for the DESIS footprint, for winter and summer pastures, and for June and August, respectively.

NDVI trend Area	June		August	
	Positive trend [%]	Negative trend [%]	Positive trend [%]	Negative trend [%]
Azerbaijan	11.1	3.8	10.4	4.9
Grassland	11.2	3.0	9.7	3.6
Cropland	11.1	4.3	10.8	5.6
Sparsely vegetated	9.2	5.5	11.3	7.6
DESI footprint	12.8	3.1	10.5	4.5
Grassland	9.7	2.3	6.2	3.0
Cropland	16.8	3.4	14.7	5.1
Sparsely vegetated	7.6	3.8	7.9	6.0
Summer pastures (grassland > 1600 m a.s.l.)	9.3	1.3	3.0	3.1
Winter pastures (grassland < 800 m a.s.l.)	11.8	4.1	12.5	3.8

cultivation assumedly increased over the last decades. In contrast, on the grassland areas fewer pixels with both positive or negative trends were detected compared to the national scale.

On the grasslands in the subalpine areas of Azerbaijan (above 1600 m), the share of positive trend pixels is a bit smaller compared to the entire country in June and especially in August. Negative trends could only be detected on 1.3% (3.1%) of the summer pastures in June (August). Positive NDVI trends on winter pastures located in the lowlands occur on 11.8% and 12.5% of the areas in June and August, respectively, which is similar to the country-wide average. Negative tendencies on summer pastures were detected on 4.1% (3.8%) of the area in June (August), which is a bit above the countrywide average. Regarding the dependency on topographic features, correlation analyses revealed that the NDVI trends do not correlate strongly with slope and aspect.

In [Figure 8](#), some examples of landscapes undergoing significant positive or negative NDVI trends are depicted. Positive trends in vegetation cover and/or vitality occur mostly in agricultural areas (pink signature in land cover map) which are developed using centre-pivot irrigation (upper row, pink frame) or irrigation through canals (second and third rows, grey and purple frame). The purple frame, however, also includes vast agricultural areas undergoing a negative NDVI trend (centre part of the image), which seem to be less intensively used or abandoned. Another example for areas of negative NDVI trends (fourth row, green frame) shows rather small-scale vegetation loss on the grassland and sparse vegetation areas of a talus cone in the Greater Caucasus. The dark red frame (bottom row), on the other hand, covers a dry grassland area near the Mingachevir Reservoir used as winter pasture, for which large percentages of the grassland area have negative NDVI trends.

3.3. Detection of land degradation risk hotspots

Spearman correlations between PV shares and monthly median NDVI values for 2020 are moderately high, with $r = 0.64$ for June and $r = 0.65$ August. In contrast, correlations between PV shares and the NDVI trend are lower, at $r = 0.39$ and $r = 0.34$ for June and August, respectively. As expected, correlations for NPV and BS shares are negative but very weak: NPV shows $r = -0.09$ and $r = -0.06$, and BS shows $r = -0.29$ for both months. This underpins the need to separate between open soil and dry vegetation, which is not feasible using multitemporal NDVI alone.

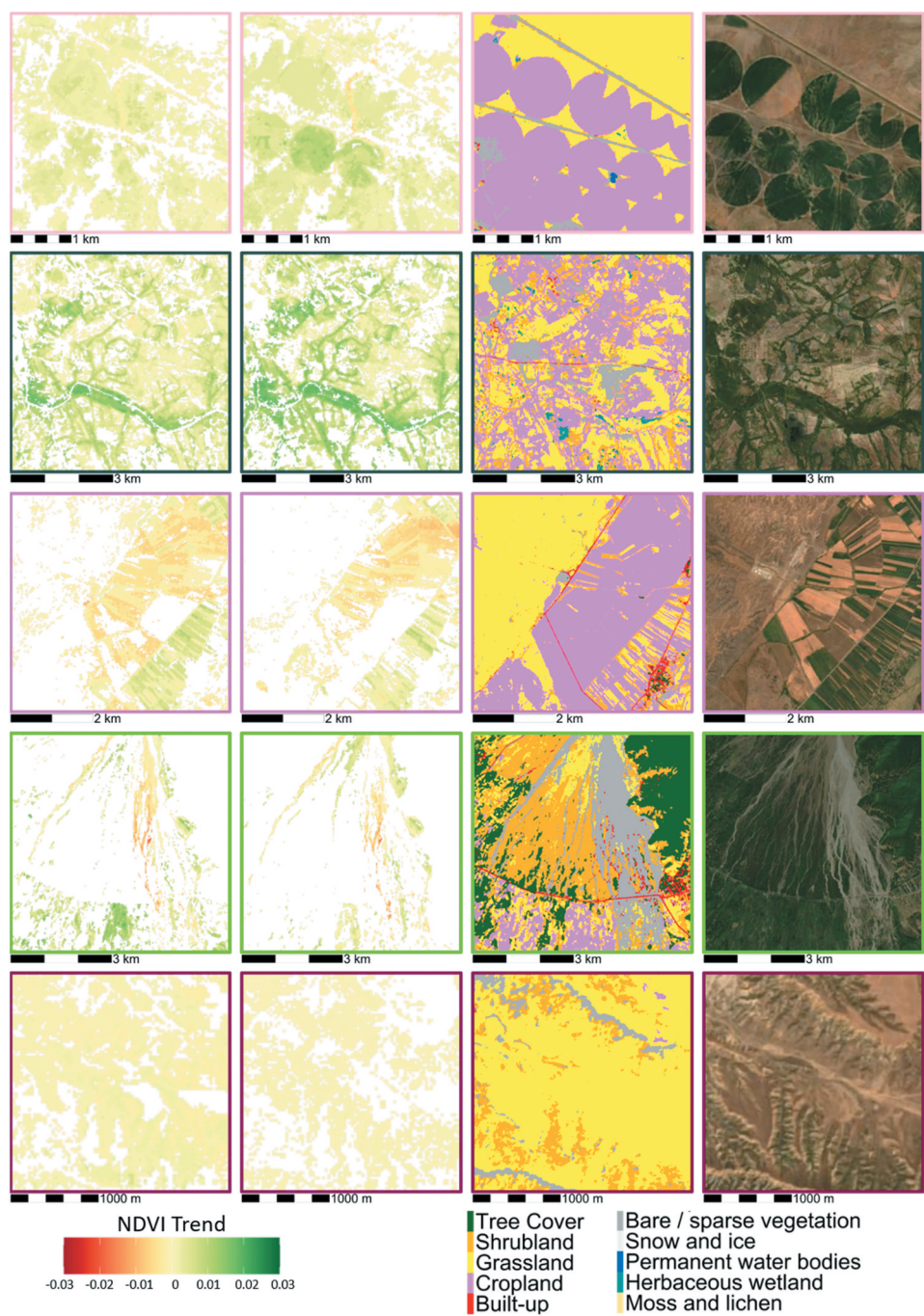


Figure 8. Landscape examples of NDVI trends. Depicted are the significant June (left) and August NDVI trends (second to left), the land cover classification (second to right) and an RGB map (right (EOX IT Services GmbH 2022) contains modified Copernicus Sentinel data 2022). Frame colours refer to the boxes shown in Figures 67 and 78.

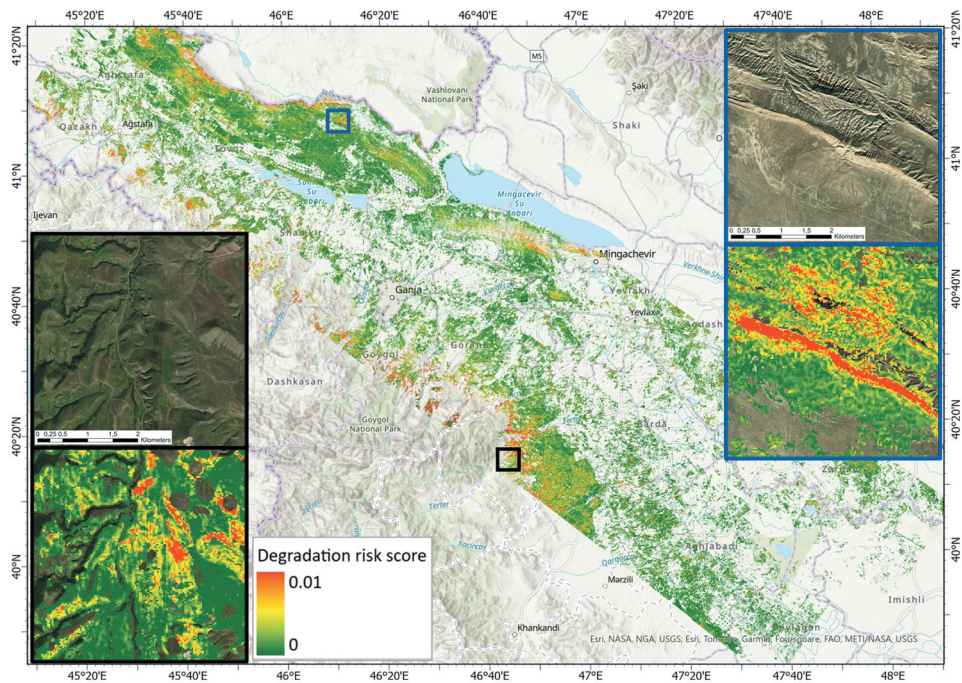


Figure 9. Land degradation risk score for the area covered by the DESIS acquisitions. The score is calculated by combining DESIS BS fCover, negative NDVI trends, and slope steepness. In the subsets, two example areas are shown in orthophotos (top), and overlaid with the risk score (bottom). Note that the value range is stretched using the standard deviation in the overview map, but as percent clip in the subsets to increase readability.

To identify hotspots of degradation risk, the results from the mono-temporal hyperspectral DESIS unmixing and the multispectral Landsat NDVI time-series trend analysis were intersected with information on slope steepness. Figure 9 displays the degradation risk map resulting from the multiplication of the scaled BS fCover, the normalized negative NDVI trend and the steepness of slope maps. The zoom windows highlight areas of high degradation risk: in orthophoto view (top) and as hotspot detection (bottom). The degradation risk score scales between 0 and 0.01, since three factors smaller than 1 are included in the calculation.

In the area of the DESIS footprint, the generated map depicts distinct patterns of degradation risk. The highest values are derived for the north-western border region of Georgia, mainly in the districts of Agstafa, and to a lesser degree in the districts of Tovuz and Samukh. An example of these sparsely vegetated steppe regions is given in the subset with the blue frame, showing a south exposed ridge near the Kura river, extensively threatened by degradation. Furthermore, the areas south of the Mingachevir Reservoir in the Yevlakh district, dominated by halophytic vegetation, show increased values. Thirdly, some areas in the northern ranges of the Lesser Caucasus exhibit increased values, mainly in the districts of Törtər and Goygol, as shown exemplary in the subset with the black frame. It zooms into a hillside area near the city of Törtər, north exposed, and

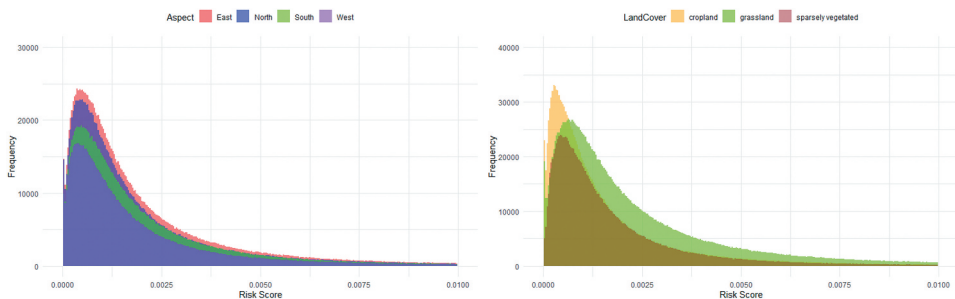


Figure 10. Distribution of degradation risk scores according to aspect (left) and land cover (right).

with rather smaller patches prone to degradation that stand out to some more intensively used, terraced grasslands in the western part of the subset.

By its nature, the degradation risk hotspot map is spatially discontinuous, since areas with no slope or positive NDVI trends are blank. In addition, there are gaps in the dataset which result mainly from missing data in the monotemporal DESIS acquisitions. For example, in the black frame subset, it can be seen that there are artificial round gaps in the risk score map, which most probably result from masked clouds and cloud shadows in the DESIS scenes. In addition, the DESIS data do not cover representatively all altitude and aspect ranges, as well as biogeographical regions of Azerbaijan. Hence, a spatial statistical analysis e.g. according to landcover or exposition cannot be exhaustive. Nevertheless, the distributions of degradation risk scores are shown in [Figure 10](#) according to aspect classes (left) and land cover classes (right). The statistical analysis shows that areas prone to degradation – in the DESIS footprint area – have a tendency to be located in grassland areas with the highest class-wise mean and median risk score values. For the aspect classes, the class-wise mean and median values are more similar, but the highest risk score values can be found on the south and east-exposed slopes.

4. Discussion

4.1. fCover mapping based on DESIS data

Seamless fCover maps could be derived for a transect over Western Azerbaijan. The mapped spatial patterns are overall reasonable, as the maps depict coherently the different landscape types and land uses in the regions of Azerbaijan, such as arid mountain ranges in the South and intensively used agricultural areas to the East. As expected for such heterogeneous environments, there are rarely pure pixels covered solely by one of the three cover types. This indicates the suitability of a subpixel approach for the highly diverse landscapes in the Caucasus region, and the added value of fCover estimates for characterizing vegetation structures in complex landscapes.

PV fractions could be derived with a MAE of 7.1%. This level of agreement between the unmixing results and in-situ data is in the range of comparable studies (Asner and Lobell 2000; Bachmann 2007; Roberts et al. 1998). General validation results for DESIS unmixing during the development of the processor gave an expected RSME of ~8% for PV based on synthetic scenes (Marshall et al. 2021). This demonstrates the general applicability of the

DESIS data for PV fCover estimation. Regarding the per-pixel abundance values, it is, however, worth pointing out that the unmixing sum-to-one criterion is often not strictly fulfilled. This indicates that to the extent of multiple DESIS tiles, the detected EMs do not fully represent the high spectral variability of such a large dataset. When no perfect knowledge of all EMs exists, the unmixing results are not always distinct or precise, and – depending on the solver – the constraints cannot be strictly fulfilled. Additional noise or multiple scattering effects measured by the sensor add to this problem. Furthermore, the spectral similarity of different EMs or the spectral variability within one EM class are expected to have an impact on the unmixing results (Bachmann 2007). All this adds to uncertainty in the estimated fCover. Nevertheless, the introduction of a shade component mitigates parts of this effect, as for the resulting abundance maps, this component is used for re-scaling (Garcia and Ustin 2001). To further improve the results, additionally, the usage of EM bundles is currently being investigated (Kühl et al. 2024).

The fCover method used in this study was successfully applied to DESIS data before (Marshall et al. 2021), and the results for PV fCover in this study are promising. However, the used fCover method was originally developed for hyperspectral sensors covering the full VNIR-SWIR range. In the case of DESIS, the spectral range is limited to 1000 nm. It is therefore important to mention that the identification of NPV is challenging, as the separation of NPV and BS can be best achieved using the absorption features of clay (~2200 nm) for BS and ligno-cellulose (~2090 nm) for NPV, which are both not covered by DESIS. Below 1000 nm, the distinction of these two classes relies on less diagnostic features. Consequently, DESIS data are expected to lead to higher confusion between EMs and to less accurate estimations of the BS and NPV fCover.

Hence, although the evaluation metrics are in a range that could be expected, some uncertainties remain when interpreting the result. In particular, the validation of the DESIS unmixing result using in-situ field data needs to be seen critically. Overall, only a small share of the collected field data could be used to assess the unmixing result, and on the remaining plots, the in-situ PV fCover data do not cover a wide range (mostly below 25%). This is caused by the circumstance, that plots of grassland with higher density could only be sampled in other regions of Azerbaijan, for which no DESIS data are available. This hampers the evidence of reliable PV estimates for more productive grasslands. Furthermore, field data were not collected during the sensor flyover but in different years and different seasons. Thereby, the seasonal mismatch might introduce higher errors, since strong changes in fCover within 2 years are not expected, but the seasonal variation of vegetation coverage can be significant. Most importantly, however, NPV and BS could not be directly validated, which is a significant limitation of the current study design. A correlation analysis between the NPV and BS shares and median NDVI indicates that the patterns of NPV and BS fCovers are reliable estimates; however, further reference data would be useful to properly quantify any errors.

Another aspect of quality is artefacts in the fCover map. As shown in Figure 11, most of the subset can be adequately modelled, with relatively low model error scores of 200–400 units and some variations on agricultural fields, likely originating from crops not perfectly represented as EMs. However, there are erroneous circular regions with high abundances in all bands. These can be related to small clouds, thin clouds and cloud shadows, which were not included in the DESIS L2A masks. As the spectra

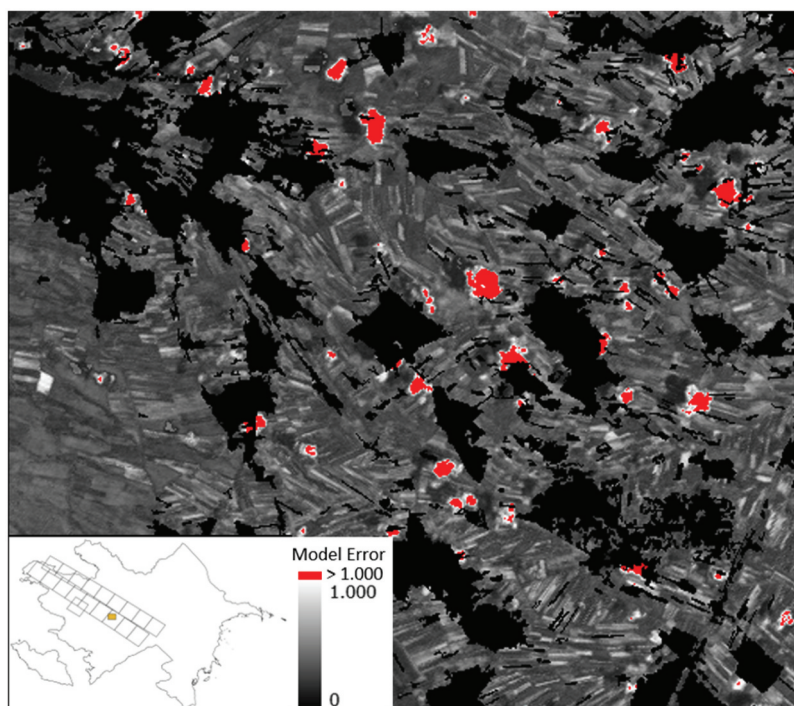


Figure 11. Unmixing model error of an example region, with a linear stretch applied and pixels with a model error above 1000 (score value) are masked in red; black areas were masked and set to background value.

of clouds are not included in the EM libraries, the pixels cannot be properly modelled, as shown by high unmixing model errors (red mask in Figure 11). These high model errors show up as artefacts in the abundance maps. Using the error score as a reliability measure, such areas can be excluded from further thematic analysis. The model error value range of the remaining areas shows that those areas can be modelled reasonably well, and no major missing EM exists which would cause high modelling errors for some local areas.

4.2. Combined use of NDVI trends and fCover for land degradation risk estimation

The presented approach aims at identifying vegetated areas prone to degradation, with a special focus on areas with decreasing vegetation vitality or abundance. To date, we are not aware of any other published study that combines NDVI trends with fCover data derived from hyperspectral data to estimate degradation risk.

High shares of BS-dominated pixels were found on the vegetated areas in the DESIS scenes, with 49% of all pixels being dominated by BS in June and 37% in August, respectively. In contrast, when looking at the NDVI trends alone, we found that only 3.8% and 4.9% of all herbaceously vegetated areas are affected by negative trends in June and August, respectively, while even smaller shares (3.0% and 3.6%) of grasslands are affected. These proportions are a bit lower than those published, for example, by

Lewińska et al. (2020), who found that 4.8% of grasslands experience decadal degradation. In contrast, our findings for summer pastures indicate negative vegetation trends for 1.3% and 3.1% of June and August areas, which is in accordance with other studies (de Leeuw et al. 2019; Shatberashvili et al. 2015), while Lewińska et al. (2020) barely detected degradation in summer pastures. It has to be mentioned, however, that they were looking at a different time span (2001–2018) and a larger region (the entire Caucasus ecoregion), which hampers a direct comparison. Nevertheless, they identified similar regions in Azerbaijan. The areas shown to be prone to degradation in our map for example, in the surroundings of the Mingachevir Reservoir and in the Aghstafa District at the border to Georgia have also been identified by Lewińska et al. (2020) to be affected by a decrease in green vegetation on decadal scales, attributing the vegetation loss of these winter pastures to overgrazing (Lewińska et al. 2020; Neudert et al. 2012; Shatberashvili et al. 2015). Furthermore, the spatial distribution of high-risk pixels in our map analysed for land cover and aspect is plausible, with grasslands in the south and east-exposed slopes, i.e. often drier slopes, are affected the most.

The suggested combination of different data sources hence leads to realistic results. In fact, PV correlates only moderately with the June median NDVI (Spearman $r = 0.64$), and with the August median NDVI ($r = 0.65$). This implies that general patterns are similar, but that a certain part of the PV fCover variance cannot be explained by NDVI. Hence, there is complementary information in fCover and vegetation indices, which depend on different vegetation parameters (i.e. woody and NPV parts, leaf area and total biomass). This further strengthens the assumption that not every sparsely vegetated area is subject to vegetation cover reduction. At the same time, a negative NDVI signal does not necessarily imply that vegetation degradation has occurred. The negative trend, especially in the end of August acquisition, could, for example, be a consequence of shifted phenology (e.g. earlier plant senescence) due to climate change. This highlights the need for such complementary datasets including information on temporal vegetation development and detailed canopy characteristics. Furthermore, correlation analyses revealed that in Azerbaijan the NDVI trends do not correlate strongly with topographic features. Therefore, it can be assumed not only that including slope and NDVI trend information does convey redundant information but also that spatial patterns beyond topography, including information on vegetation development, could be generated. Nonetheless, we recognize the value of more systematic sensitivity analyses and plan to investigate the individual and combined influences of each variable in the future work.

Based on the resulting map, it is now possible to identify hotspots prone to degradation to take up early measures and prevent loss of valuable top soil. For example, agricultural planning tools such as the proper use factor that is needed for the estimation of the livestock carrying capacity, especially in the Caucasus region, but often lack the information of vegetation ground cover (de Leeuw et al. 2019). It would be interesting to test the approach at different biogeographical regions. Since no threshold or categories have been introduced, the concept is easily transferable.

However, some limitations of the approach have to be considered. First, we did not consider any land cover changes due to the lack of appropriate datasets from the 1990s. This most probably introduces errors, since land cover changes e.g. from cropland/grassland abandonment, might result in a negative NDVI trend simply from changing species composition. While this issue cannot be solved for the investigated study area, it could be

accounted for when transferring the approach to areas with more consistent information on land cover changes, e.g. from the Copernicus Land Monitoring Service. Furthermore, the issue of spatial resolution should be mentioned. 30 m spatial resolution might be too coarse in some small-scaled landscapes in the Caucasus region with its rugged relief and small fields. While subpixel mapping is generally a good approach for heterogeneous landscapes, the spectral unmixing process and therewith the fCover estimation could still be hampered, e.g. if small landscape elements such as bushes, hedges, roads or canals are not sufficiently differentiated and captured in EMs, or properly masked. Furthermore, variations in vegetation cover relevant for degradation processes especially in mountainous terrain (for example, through trampling trails or gullies (Neudert et al. 2012)) occur within a few metres, which might be too small-scaled to be represented prominently in the BS fCover component. Last but not least, the map generated through the combined use of DESIS data and Landsat time series looks plausible but could not be validated through the available in situ data.

While the suggested approach of this study generates realistic results and proves the added value of fCover estimates for the assessment of land degradation, its intersection of independent datasets is both practicable and easily transferable, and a few options could be considered to further improve the degradation hotspot identification. For example, fCover at several time steps, for several years and also at several stages throughout the phenological growing cycle, would be useful for a detailed degradation risk estimate, as well as to avoid gaps, and would be a logical extension of the current study (see e.g. Soto et al. 2024). Time series from DESIS and other hyperspectral sensors (e.g. EnMAP (Chabrillat et al. 2024; Storch et al. 2023) and PRISMA (Cogliati et al. 2021)) are now and in the future (e.g. through missions like CHMIE (Buschkamp et al. 2023)) becoming more and more available and provide a valuable data source for informed degradation risk monitoring. Furthermore, the analysis of multispectral time series could be further enriched by assessing phenological parameters (Chen et al. 2018) or enriching the fCover time series (Kowalski et al. 2022; Lewińska et al. 2021).

5. Conclusions

Land degradation, driven by climate change and land use pressures, significantly impacts mountain ecosystems, particularly in arid regions, leading to reduced vegetation cover and increased soil erosion. Effective monitoring is essential for identifying degradation and managing risks through sustainable land management. In this study, we combined hyperspectral DESIS data with long-term NDVI time series from Landsat (1987–2021) to assess vegetation degradation in Azerbaijan. We derived PV fractions with a MAE of 7.1%, demonstrating that DESIS is effective for estimating vegetation cover, even without the SWIR range. By intersecting BS fCover with negative NDVI trends and slope steepness, we generated a degradation risk map, highlighting degradation hotspots on grassland areas mainly on south-facing slopes. Integrating NDVI trends with fCover estimates hence provided an improved assessment of land degradation, offering insights into vegetation dynamics beyond what either dataset could provide alone. However, limitations include the lack of ground data for validating NPV and BS fCovers, which restricts the assessment of how well these fractions are differentiated and limits the evaluation of degradation risks. Despite these challenges,

our study demonstrates the potential of combining hyperspectral and multispectral data to enhance land management, such as by improving livestock carrying capacity estimates in mountainous grasslands. With the increasing availability of time series data from sensors like DESIS and EnMAP, this approach can be refined to deliver more accurate and dynamic assessments of vegetation health and degradation risk. In conclusion, integrating long-term vegetation trends with detailed cover fraction mapping is a valuable tool for detecting land degradation and supporting sustainable land management strategies.

Acknowledgements

The DESIS ground segment at DLR and Teledyne Brown Engineering are acknowledged for providing the DESIS data. Landsat image courtesy of the U.S. Geological Survey. We thank Tobias Köstl and Daniel Wuttej from the E.C.O. Institute for the collection of the field data. We thank three anonymous reviewers whose comments significantly improved the quality of the paper.

Disclosure statement

No potential conflict of interest was reported by the author(s).

Data availability statement

Landsat NDVI time series and degradation risk maps are available upon request by contacting the corresponding author. DESIS scenes can be accessed for scientific purposes from the archive at <https://eoweb.dlr.de/egp/>.

ORCID

Sarah Asam  <http://orcid.org/0000-0002-7302-6813>

Frederic Schwarzenbacher  <http://orcid.org/0000-0003-1173-386X>

David Marshall Ingram  <http://orcid.org/0000-0002-4765-8198>

Martin Bachmann  <http://orcid.org/0000-0001-8381-7662>

References

- Abdolzadeh, Z., A. Ghorbani, R. Mostafazadeh, and M. Moameri. 2020. "Rangeland Canopy Cover Estimation Using Landsat OLI Data and Vegetation Indices in Sabalan Rangelands, Iran." *Arabian Journal of Geosciences* 13 (6): 245. <https://doi.org/10.1007/s12517-020-5150-1>.
- Akhmadov, K. M., S. W. Breckle, and U. Breckle. 2006. "Effects of Grazing on Biodiversity, Productivity, and Soil Erosion of Alpine Pastures in Tajik Mountains." In *Land Use Change and Mountain Biodiversity*, edited by E. M. Spehn, M. Liberman, and C. Körner, 376. Boca Raton: CRC Press.
- Akiyama, T., and K. Kawamura. 2007. "Grassland Degradation in China: Methods of Monitoring, Management and Restoration." *Grassland Science* 53 (1): 1–17. <https://doi.org/10.1111/j.1744-697X.2007.00073.x>.
- Ali, I., F. Cawkwell, E. Dwyer, B. Barrett, and S. Green. 2016. "Satellite Remote Sensing of Grasslands: From Observation to Management." *Journal of Plant Ecology* 9 (6): 649–671. <https://doi.org/10.1093/jpe/rtw005>.

- Alonso, K., M. Bachmann, K. Burch, E. Carmona, D. Cerra, R. de Los Reyes, D. Dietrich, et al. 2019. "Data Products, Quality and Validation of the DLR Earth Sensing Imaging Spectrometer (DESI)." *Sensors (Switzerland)* 19 (20). <https://doi.org/10.3390/s19204471>.
- Aneece, I., D. Foley, P. Thenkabail, A. Oliphant, and P. Teluguntla. 2022. "New Generation Hyperspectral Data from DESIS Compared to High Spatial Resolution Planetscope Data for Crop Type Classification." *IEEE Journal of Selected Topics in Applied Earth Observations & Remote Sensing* 15:7846–7858. <https://doi.org/10.1109/jstars.2022.3204223>.
- Aneece, I., and P. S. Thenkabail. 2021. "Classifying Crop Types Using Two Generations of Hyperspectral Sensors (Hyperion and DESIS) with Machine Learning on the Cloud." *Remote Sensing* 13 (22). <https://doi.org/10.3390/rs13224704>.
- Arsenault, É., and F. Bonn. 2005. "Evaluation of Soil Erosion Protective Cover by Crop Residues Using Vegetation Indices and Spectral Mixture Analysis of Multispectral and Hyperspectral Data." *Catena* 62 (2): 157–172. <https://doi.org/10.1016/j.catena.2005.05.003>.
- Asam, S., C. Eisfelder, A. Hirner, P. Reiners, S. Holzwarth, and M. Bachmann. 2023. "AVHRR NDVI Compositing Method Comparison and Generation of Multi-Decadal Time Series—A TIMELINE Thematic Processor." *Remote Sensing* 15 (6): 1631. <https://doi.org/10.3390/rs15061631>.
- Asner, G. P. 1998. "Biophysical and Biochemical Sources of Variability in Canopy Reflectance." *Remote Sensing of Environment* 64 (3): 234–253. [https://doi.org/10.1016/S0034-4257\(98\)00014-5](https://doi.org/10.1016/S0034-4257(98)00014-5).
- Asner, G. P., and D. B. Lobell. 2000. "A Biogeophysical Approach for Automated SWIR Unmixing of Soils and Vegetation." *Remote Sensing of Environment* 74 (1): 99–112. [https://doi.org/10.1016/S0034-4257\(00\)00126-7](https://doi.org/10.1016/S0034-4257(00)00126-7).
- Bachmann, M. 2007. *Automated Estimation of Ground Cover Fractions Using MESMA Unmixing*. Universität Würzburg Dissertation.
- Bachmann, M., A. Muller, and S. Dech. 2009. "Increasing and Evaluating the Reliability of Multiple Endmember Spectral Mixture Analysis (MESMA)." Paper presented at the 6th EARSeL-SIG-IS, Tel Aviv, Israel: 16.–18. März 2009.
- Bai, Z. G., D. L. Dent, L. Olsson, and M. E. Schaepman. 2008. "Proxy Global Assessment of Land Degradation." *Soil Use and Management* 24 (3): 223–234. <https://doi.org/10.1111/j.1475-2743.2008.00169.x>.
- Bayer, A. D., M. Bachmann, D. Rogge, A. Müller, and H. Kaufmann. 2016. "Combining Field and Imaging Spectroscopy to Map Soil Organic Carbon in a Semi-arid Environment." *IEEE Journal of Selected Topics in Applied Earth Observations & Remote Sensing* 9 (9): 3997–4010. <https://doi.org/10.1109/jstars.2016.2585674>.
- Bengtsson, J., J. M. Bullock, B. Egoh, C. Everson, T. Everson, T. O'Connor, P. J. O'Farrell, H. G. Smith, and R. Lindborg. 2019. "Grasslands—More Important for Ecosystem Services Than You Might Think." *Ecosphere* 10 (2): e02582. <https://doi.org/10.1002/ecs2.2582>.
- Borchardt, P., U. Schickhoff, S. Scheitweiler, and M. Kulikov. 2011. "Mountain Pastures and Grasslands in the SW Tien Shan, Kyrgyzstan — Floristic Patterns, Environmental Gradients, Phytogeography, and Grazing Impact." *Journal of Mountain Science* 8 (3): 363–373. <https://doi.org/10.1007/s11629-011-2121-8>.
- Braaten, J. 2024. "Landsat ETM+ to OLI Harmonization." Google. Accessed May 23, 2025. <https://developers.google.com/earth-engine/tutorials/community/landsat-etm-to-oli-harmonization>.
- Bracken, A., C. Coburn, K. Staez, N. Rochdi, K. Segl, S. Chabrillat, and T. Schmid. 2019. "Detecting Soil Erosion in Semi-Arid Mediterranean Environments Using Simulated EnMAP Data." *Geoderma* 340:164–174. <https://doi.org/10.1016/j.geoderma.2019.01.026>.
- Buchner, J., H. Yin, D. Frantz, T. Kuemmerle, E. Askerov, T. Bakuradze, B. Bleyhl, et al. 2020. "Land-Cover Change in the Caucasus Mountains Since 1987 Based on the Topographic Correction of Multi-Temporal Landsat Composites." *Remote Sensing of Environment* 248:111967. <https://doi.org/10.1016/j.rse.2020.111967>.
- Buschkamp, P., J. Hofmann, D. Rio-Fernandes, P. Haberler, M. Gerstmeier, C. Bartscher, S. Bianchi, et al. 2023. "CHIME's Hyperspectral Imager (HSI): Status of Instrument Design and Performance at PDR." *International Conference on Space Optics — ICSO 2022*. Vol. 12777. SPIE.
- Campbell, P. E. K., K. F. Huemmrich, E. M. Middleton, J. Alfieri, C. van Der Tol, and C. S. R. Neigh. 2021. "Using DESIS and EO-1 Hyperion Reflectance Time Series for the Assessment of Vegetation Traits

- and Gross Primary Production (GPP)." 1st DESIS User Workshop on Imaging Spectrometer Space Mission, Calibration and Validation, Applications, Methods Sep28-Oct 01 2021 virtual event.
- Carmona, E., K. Alonso, M. Bachmann, K. Burch, D. Cerra, R. Reyes, U. Heiden, et al. 2022. "Vicarious Calibration of the Desis Imaging Spectrometer: Status and Plans." *IGARSS 2022 - 2022 IEEE International Geoscience and Remote Sensing Symposium* 17-22 July 2022 Kuala Lumpur, Malaysia, 4587–4590.
- Chabrilat, S., S. Foerster, K. Segl, A. Beamish, M. Brell, S. Asadzadeh, R. Milewski, et al. 2024. "The enmap Spaceborne Imaging Spectroscopy Mission: Initial Scientific Results Two Years After Launch." *Remote Sensing of Environment* 315:114379. <https://doi.org/10.1016/j.rse.2024.114379>.
- Chen, H., X. Liu, C. Ding, and F. Huang. 2018. "Phenology-Based Residual Trend Analysis of MODIS–NDVI Time Series for Assessing Human-Induced Land Degradation." *Sensors (Switzerland)* 18 (11): 3676.
- Cogliati, S., F. Sarti, L. Chiarantini, M. Cosi, R. Lorusso, E. Lopinto, F. Miglietta, et al. 2021. "The PRISMA Imaging Spectroscopy Mission: Overview and First Performance Analysis." *Remote Sensing of Environment* 262:112499. <https://doi.org/10.1016/j.rse.2021.112499>.
- Conant, R. T., C. E. P. Cerri, B. B. Osborne, and K. Paustian. 2017. "Grassland Management Impacts on Soil Carbon Stocks: A New Synthesis." *Ecological Applications* 27 (2): 662–668. <https://doi.org/10.1002/eap.1473>.
- Conant, R. T., and K. Paustian. 2002. "Potential Soil Carbon Sequestration in Overgrazed Grassland Ecosystems." *Global Biogeochemical Cycles* 16 (4): 90–91. <https://doi.org/10.1029/2001GB001661>.
- Cooper, S., A. Okujeni, C. Jänicke, M. Clark, S. van der Linden, and P. Hostert. 2020. "Disentangling Fractional Vegetation Cover: Regression-Based Unmixing of Simulated Spaceborne Imaging Spectroscopy Data." *Remote Sensing of Environment* 246:111856. <https://doi.org/10.1016/j.rse.2020.111856>.
- D'Acunto, F., F. Marinello, and A. Pezzuolo. 2024. "Rural Land Degradation Assessment Through Remote Sensing: Current Technologies, Models, and Applications." *Remote Sensing* 16 (16): 3059.
- de Leeuw, J., A. Rizayeva, E. Namazov, E. Bayramov, M. T. Marshall, J. Etzold, and R. Neudert. 2019. "Application of the MODIS MOD 17 Net Primary Production Product in Grassland Carrying Capacity Assessment." *International Journal of Applied Earth Observation and Geoinformation* 78:66–76. <https://doi.org/10.1016/j.jag.2018.09.014>.
- Dennison, P. E., and D. A. Roberts. 2003. "Endmember Selection for Multiple Endmember Spectral Mixture Analysis Using Endmember Average RMSE." *Remote Sensing of Environment* 87 (2): 123–135. [https://doi.org/10.1016/S0034-4257\(03\)00135-4](https://doi.org/10.1016/S0034-4257(03)00135-4).
- Dubovyk, O. 2017. "The Role of Remote Sensing in Land Degradation Assessments: Opportunities and Challenges." *European Journal of Remote Sensing* 50 (1): 601–613. <https://doi.org/10.1080/22797254.2017.1378926>.
- E.C.O. Institut für Ökologie Jungmeier GmbH 2023. "E.C.O. Institute of Ecology - Nature Conservation in the 21st Century." Accessed February 22, 2023. <https://e-c-o.at/home-en.html>.
- EOX IT Services GmbH. 2022. *Sentinel-2 Cloudless 2022*, In. <https://s2maps.eu>.
- Farr, T. G., P. A. Rosen, E. Caro, R. Crippen, R. Duren, S. Hensley, M. Kobrick, et al. 2007. "The Shuttle Radar Topography Mission." *Reviews of Geophysics* 45 (2). <https://doi.org/10.1029/2005RG000183>.
- Fava, F., R. Colombo, S. Bocchi, and C. Zucca. 2012. "Assessment of Mediterranean Pasture Condition Using MODIS Normalized Difference Vegetation Index Time Series." *Journal of Applied Remote Sensing* 6 (1): 063530. <https://doi.org/10.1117/1.JRS.6.063530>.
- Gamon, J. A., J. Peñuelas, and C. B. Field. 1992. "A Narrow-Waveband Spectral Index That Tracks Diurnal Changes in Photosynthetic Efficiency." *Remote Sensing of Environment* 41 (1): 35–44. [https://doi.org/10.1016/0034-4257\(92\)90059-S](https://doi.org/10.1016/0034-4257(92)90059-S).
- García-Haro, F. J., S. Sommer, and T. Kemper. 2005. "A New Tool for Variable Multiple Endmember Spectral Mixture Analysis (VMESMA)." *International Journal of Remote Sensing* 26 (10): 2135–2162. <https://doi.org/10.1080/01431160512331337817>.
- Garcia, M., and S. L. Ustin. 2001. "Detection of Interannual Vegetation Responses to Climatic Variability Using AVIRIS Data in a Coastal Savanna in California." *IEEE Transactions on Geoscience & Remote Sensing* 39 (7): 1480–1490. <https://doi.org/10.1109/36.934079>.

- Gholizadeh, H., A. P. Dixon, K. H. Pan, N. A. McMillan, R. G. Hamilton, S. D. Fuhlendorf, J. Cavender-Bares, and J. A. Gamon. 2022. "Using Airborne and DESIS Imaging Spectroscopy to Map Plant Diversity Across the Largest Contiguous Tract of Tallgrass Prairie on Earth." *Remote Sensing of Environment* 281:16. <https://doi.org/10.1016/j.rse.2022.113254>.
- Gorelick, N., M. Hancher, M. Dixon, S. Ilyushchenko, D. Thau, and R. Moore. 2017. "Google Earth Engine: Planetary-Scale Geospatial Analysis for Everyone." *Remote Sensing of Environment* 202:18–27. <https://doi.org/10.1016/j.rse.2017.06.031>.
- Guerschman, J. P., P. F. Scarth, T. R. McVicar, L. J. Renzullo, T. J. Malthus, J. B. Stewart, J. E. Rickards, and R. Trevithick. 2015. "Assessing the Effects of Site Heterogeneity and Soil Properties When Unmixing Photosynthetic Vegetation, Non-Photosynthetic Vegetation and Bare Soil Fractions from Landsat and MODIS Data." *Remote Sensing of Environment* 161:12–26. <https://doi.org/10.1016/j.rse.2015.01.021>.
- Guo, Z., Y. Xie, H. Guo, X. Zhang, G. Xi, C. Ma, and H. Duan. 2023. "Is Land Degradation Worsening in Northern China? Quantitative Evidence and Enlightenment from Satellites." *Land Degradation & Development* 34 (6): 1662–1680. <https://doi.org/10.1002/ldr.4560>.
- Gyssels, G., J. Poesen, E. Bochet, and Y. Li. 2005. "Impact of Plant Roots on the Resistance of Soils to Erosion by Water: A Review." *Progress in Physical Geography: Earth and Environment* 29 (2): 189–217. <https://doi.org/10.1191/0309133305pp443ra>.
- Hernández-Clemente, R., A. Hornero, V. Gonzalez-Dugo, M. Berdugo, J. L. Quero, J. C. Jiménez, and F. T. Maestre. 2023. "Global Monitoring of Soil Multifunctionality in Drylands Using Satellite Imagery and Field Data." *Remote Sensing in Ecology and Conservation* 9 (6): 743–758. <https://doi.org/10.1002/rse2.340>.
- Huemmrich, K. F., P. E. K. Campbell, D. J. Harding, K. J. Ranson, R. Wynne, V. Thomas, and E. M. Middleton. 2021. "Evaluating Approaches Relating Ecosystem Productivity with DESIS Spectral Information." 1st DESIS User Workshop on Imaging Spectrometer Space Mission, Calibration and Validation, Applications, Methods Sep28-Oct 01 2021 virtual event.
- Iniguez, L., M. Suleimenov, S. Yusupov, A. Ajibekov, M. Kineev, S. Kheremov, A. Abdusattarov, D. Thomas, and M. Musaeva. 2005. "Livestock Production in Central Asia: Constraints and Opportunities." *ICARDA Caravan* :22 18–22.
- Ismayilov, A. I., A. I. Mamedov, H. Fujimaki, A. Tsunekawa, and G. J. Levy. 2021. "Soil Salinity Type Effects on the Relationship Between the Electrical Conductivity and Salt Content for 1: 5 Soil-To-Water Extract." *Sustainability* 13 (6): 3395. <https://doi.org/10.3390/su13063395>.
- Kamaraj, N. P., H. Gholizadeh, R. G. Hamilton, S. D. Fuhlendorf, and J. A. Gamon. 2024. "Estimating Plant β -Diversity Using Airborne and Spaceborne Imaging Spectroscopy." *International Journal of Remote Sensing*: 1–20. <https://doi.org/10.1080/01431161.2024.2410959>.
- Kang, J., Y. Zhang, and A. Biswas. 2021. "Land Degradation and Development Processes and Their Response to Climate Change and Human Activity in China from 1982 to 2015." *Remote Sensing* 13 (17): 3516. <https://doi.org/10.3390/rs13173516>.
- Karlen, D. L., S. S. Andrews, B. J. Weinhold, and J. W. Doran. 2003. "Soil Quality: Humankind's Foundation for Survival." *Journal of Soil and Water Conservation* 58 (4): 171–179. <https://doi.org/10.1080/00224561.2003.12457524>.
- Kendall, M. 1975. *Rank Correlation Measures*. Vol. 202. London: Charles Griffin.
- Köstl, T., D. Wuttej, and H. Kirchmeir. 2018. *Integrated Biodiversity Management in South Caucasus – Collection of Field Data in Azerbaijan*. Vol. 11. Klagenfurt: E.C.O. Institut of Ecology.
- Kowalski, K., A. Okujeni, M. Brell, and P. Hostert. 2022. "Quantifying Drought Effects in Central European Grasslands Through Regression-Based Unmixing of Intra-Annual Sentinel-2 Time Series." *Remote Sensing of Environment* 268:112781. <https://doi.org/10.1016/j.rse.2021.112781>.
- Krutz, D., R. Müller, U. Knodt, B. Günther, I. Walter, I. Sebastian, T. Säuberlich, et al. 2019. "The Instrument Design of the DLR Earth Sensing Imaging Spectrometer (DESI)." *Sensors (Switzerland)* 19 (7): 1622. <https://doi.org/10.3390/s19071622>.
- Kühl, K., D. Marshall Ingram, U. Heiden, and M. Bachmann. 2024. "Creating Temporal Hyperspectral Regional Endmember Bundles (THREBs): Automatic Imaged Based EM Extraction and Library Reduction to Derive Regional Fractional Vegetation Cover." *13th EARSeL Workshop on Imaging Spectroscopy*, Valencia, Spain.

- Le, Q. B., L. Tamene, and P. L. G. Vlek. 2012. "Multi-Pronged Assessment of Land Degradation in West Africa to Assess the Importance of Atmospheric Fertilization in Masking the Processes Involved." *Global and Planetary Change* 92-93:71–81. <https://doi.org/10.1016/j.gloplacha.2012.05.003>.
- Lewińska, K. E., J. Buchner, B. Bleyhl, P. Hostert, H. Yin, T. Kuemmerle, and V. C. Radeloff. 2021. "Changes in the Grasslands of the Caucasus Based on Cumulative Endmember Fractions from the Full 1987–2019 Landsat Record." *Science of Remote Sensing* 4:100035. <https://doi.org/10.1016/j.srs.2021.100035>.
- Lewińska, K. E., P. Hostert, J. Buchner, B. Bleyhl, and V. C. Radeloff. 2020. "Short-Term Vegetation Loss versus Decadal Degradation of Grasslands in the Caucasus Based on Cumulative Endmember Fractions." *Remote Sensing of Environment* 248:111969. <https://doi.org/10.1016/j.rse.2020.111969>.
- Lewińska, K. E., A. Okujeni, K. Kowalski, F. Lehmann, V. C. Radeloff, U. Leser, and P. Hostert. 2025. "Impact of Data Density and Endmember Definitions on Long-Term Trends in Ground Cover Fractions Across European Grasslands." *Remote Sensing of Environment* 323. <https://doi.org/10.1016/j.rse.2025.114736>.
- Li, Z., and X. Guo. 2016. "Remote Sensing of Terrestrial Non-Photosynthetic Vegetation Using Hyperspectral, Multispectral, SAR, and lidar Data." *Progress in Physical Geography: Earth and Environment* 40 (2): 276–304. <https://doi.org/10.1177/0309133315582005>.
- Liu, B., W. Shen, N. Lin, R. Li, and Y. Yue. 2014. "Deriving Vegetation Fraction Information for the Alpine Grassland on the Tibetan Plateau Using in situ Spectral Data." *Journal of Applied Remote Sensing* 8:083630. <https://doi.org/10.1117/1.JRS.8.083630>.
- Liu, B., G. You, R. Li, W. Shen, Y. Yue, and N. Lin. 2015. "Spectral Characteristics of Alpine Grassland and Their Changes Responding to Grassland Degradation on the Tibetan Plateau." *Environmental Earth Sciences* 74 (3): 2115–2123. <https://doi.org/10.1007/s12665-015-4196-y>.
- Lyu, X., X. Li, D. Dang, H. Dou, X. Xuan, S. Liu, M. Li, and J. Gong. 2020. "A New Method for Grassland Degradation Monitoring by Vegetation Species Composition Using Hyperspectral Remote Sensing." *Ecological Indicators* 114:106310. <https://doi.org/10.1016/j.ecolind.2020.106310>.
- Mafanya, M., P. Tsele, T. Zengeya, and A. Ramoelo. 2022. "An Assessment of Image Classifiers for Generating Machine-Learning Training Samples for Mapping the Invasive *Campuloclinium Macrocephalum* (less.) DC (Pompom Weed) Using DESIS Hyperspectral Imagery." *Isprs Journal of Photogrammetry & Remote Sensing* 185:188–200. <https://doi.org/10.1016/j.isprsjprs.2022.01.015>.
- Magiera, A., H. Feilhauer, A. Otte, R. Waldhardt, and D. Simmering. 2013. "Relating Canopy Reflectance to the Vegetation Composition of Mountainous Grasslands in the Greater Caucasus." *Agriculture, Ecosystems & Environment* 177:101–112. <https://doi.org/10.1016/j.agee.2013.05.017>.
- Malec, S., D. Rogge, U. Heiden, A. Sanchez-Azofeifa, M. Bachmann, and M. Wegmann. 2015. "Capability of Spaceborne Hyperspectral enmap Mission for Mapping Fractional Cover for Soil Erosion Modeling." *Remote Sensing* 7 (9): 11776–11800. <https://doi.org/10.3390/rs70911776>.
- Mann, H. B. 1945. "Nonparametric Tests Against Trend." *Econometrica* 13 (3). <https://doi.org/10.2307/1907187>.
- Marshall, D., M. Bachmann, M. Habermeyer, U. Heiden, S. Holzwarth, and T. Schmid. 2021. "An Automated Operational Processor for the Determination of Fractional Vegetation Cover from DESIS Observations." 1st DESIS User Workshop on Imaging Spectrometer Space Mission, Calibration and Validation, Applications, Methods 28. Sept - 01. Oct.2021 Virtual event.
- Masek, J. G., E. F. Vermote, N. E. Saleous, R. Wolfe, F. G. Hall, K. F. Huemmrich, F. Gao, J. Kutler, and T.-K. Lim. 2006. "A Landsat Surface Reflectance Dataset for North America, 1990-2000." *IEEE Geoscience & Remote Sensing Letters* 3 (1): 68–72. <https://doi.org/10.1109/LGRS.2005.857030>.
- Milchunas, D. G., and W. K. Lauenroth. 1993. "Quantitative Effects of Grazing on Vegetation and Soils Over a Global Range of Environments." *Ecological Monographs* 63 (4): 327–366. <https://doi.org/10.2307/2937150>.
- Nagler, P. L., C. S. T. Daughtry, and S. N. Goward. 2000. "Plant Litter and Soil Reflectance." *Remote Sensing of Environment* 71 (2): 207–215. [https://doi.org/10.1016/S0034-4257\(99\)00082-6](https://doi.org/10.1016/S0034-4257(99)00082-6).

- Neudert, R., J. Etzold, F. Münzner, M. Manthey, and S. Busse. 2012. "The Opportunity Costs of Conserving Pasture Resources for Mobile Pastoralists in the Greater Caucasus." *Landscape Research* 38 (4): 499–522. <https://doi.org/10.1080/01426397.2012.728204>.
- Obermeier, W. A., L. W. Lehnert, M. J. Pohl, S. Makowski Gianonni, B. Silva, R. Seibert, H. Laser, et al. 2019. "Grassland Ecosystem Services in a Changing Environment: The Potential of Hyperspectral Monitoring." *Remote Sensing of Environment* 232:111273. <https://doi.org/10.1016/j.rse.2019.111273>.
- Olsson, L., H. Barbosa, S. Bhadwal, A. Cowie, K. Delusca, D. Flores-Renteria, K. Hermans, V. Masson-Delmotte, H.-O. Pörtner, D. C. Roberts, P. Zhai, et al. 2019. "Land Degradation." In *Climate Change and Land: An IPCC Special Report on Climate Change, Desertification, Land Degradation, Sustainable Land Management, Food security, And Greenhouse Gas Fluxes in Terrestrial Ecosystems* doi:10.1017/9781009157988.006, edited by P. R. Shukla, J. Skea, and E. C. Buendia, Masson-Delmotte, V., Pörtner, H.-O., Roberts, D. C., Zhai, P., Slade, R., Connors, S., van Diemen, R., Ferrat, M., Haughey, E., Luz, S., Neogi, S., Pathak, M., Petzold, J., Portugal Pereira, J., Vyas, P., Huntley, E., Kissick, K., Belkacemi, M. editors.
- Pacheco-Labrador, J., M. Migliavacca, X. L. Ma, M. Mahecha, N. Carvalhais, U. Weber, R. Benavides, et al. 2022. "Challenging the Link Between Functional and Spectral Diversity with Radiative Transfer Modeling and Data." *Remote Sensing of Environment*: 280. <https://doi.org/10.1016/j.rse.2022.113170>.
- Pacheco-Labrador, J., U. Weber, X. Ma, M. D. Mahecha, N. Carvalhais, C. Wirth, A. Huth, et al. 2021. "Evaluating the Potential of DESIS to Infer Plant Taxionomical and Functional Diversities in European Forests." 1st DESIS User Workshop on Imaging Spectrometer Space Mission, Calibration and Validation, Applications, Methods Sep 28 - Oct 01 2021 virtual event.
- Paulik, F. 2018. *Supervised Machine Learning for Spectral Classification Using Hyperspectral Images of semi-Arid Regions*. : Ludwig-Maximilians-Universität München.
- Master thesis
- Pi, W., J. Du, Y. Bi, X. Gao, and X. Zhu. 2021. "3D-CNN Based UAV Hyperspectral Imagery for Grassland Degradation Indicator Ground Object Classification Research." *Ecological Informatics* 62:101278. <https://doi.org/10.1016/j.ecoinf.2021.101278>.
- Prince, S. D., I. Becker-Reshef, and K. Rishmawi. 2009. "Detection and Mapping of Long-Term Land Degradation Using Local Net Production Scaling: Application to Zimbabwe." *Remote Sensing of Environment* 113 (5): 1046–1057. <https://doi.org/10.1016/j.rse.2009.01.016>.
- Reeves, M. C., and L. S. Baggett. 2014. "A Remote Sensing Protocol for Identifying Rangelands with Degraded Productive Capacity." *Ecological Indicators* 43:172–182. <https://doi.org/10.1016/j.ecoind.2014.02.009>.
- Reeves, M., R. A. Washington-Allen, J. Angerer, E. R. Hunt, R. W. Kulawardhana, L. Kumar, T. Loboda, T. Loveland, G. Metternicht, and R. D. Ramsey. 2015. "Global View of Remote Sensing of Rangelands: Evolution, Applications, Future Pathways [Chapter 10] Thenkabail, P. S." In *Land Resources Monitoring, Modeling, and Mapping with Remote Sensing*, 237–276. Boca Raton, FL: CRC Press/Taylor and Francis Group.
- Roberts, D. A., M. Gardner, R. Church, S. Ustin, G. Scheer, and R. O. Green. 1998. "Mapping Chaparral in the Santa Monica Mountains Using Multiple Endmember Spectral Mixture Models." *Remote Sensing of Environment* 65 (3): 267–279. [https://doi.org/10.1016/S0034-4257\(98\)00037-6](https://doi.org/10.1016/S0034-4257(98)00037-6).
- Rogge, D., M. Bachmann, B. Rivard, and J. Feng. 2012. "Spatial Sub-Sampling Using Local Endmembers for Adapting OSP and SSEE for Large-Scale Hyperspectral Surveys." *IEEE Journal of Selected Topics in Applied Earth Observations & Remote Sensing* 5 (1): 183–195. <https://doi.org/10.1109/JSTARS.2011.2168513>.
- Rogge, D. M., B. Rivard, J. Zhang, A. Sanchez, J. Harris, and J. Feng. 2007. "Integration of Spatial-Spectral Information for the Improved Extraction of Endmembers." *Remote Sensing of Environment* 110 (3): 287–303. <https://doi.org/10.1016/j.rse.2007.02.019>.
- Roy, D. P., V. Kovalskyy, H. K. Zhang, E. F. Vermote, L. Yan, S. S. Kumar, and A. Egorov. 2016. "Characterization of Landsat-7 to Landsat-8 Reflective Wavelength and Normalized Difference Vegetation Index Continuity." *Remote Sensing of Environment* 185:57–70. <https://doi.org/10.1016/j.rse.2015.12.024>.

- Sen, P. R. 1968. "Estimates of the Regression Coefficient Based on Kendall's Tau." *Journal of the American Statistical Association* 63 (324): 1379–1389. <https://doi.org/10.1080/01621459.1968.10480934>.
- Shatberashvili, N., I. Rucevska, H. Jørstad, K. Artsivadze, B. Mehdiyev, M. Aliyev, G. Fayvush, et al. 2015. "." In *Outlook on Climate Change Adaptation in the South Caucasus Mountains Mountain Adaptation Outlook Series*, Nairobi, Arendal and Tbilisi: United Nations Environment Programme, GRID-Arendal and Sustainable Caucasus. Nairobi 88.
- Soto, G. E., S. W. Wilcox, P. E. Clark, F. P. Fava, N. D. Jensen, N. Kahiu, C. Liao, B. Porter, Y. Sun, and C. B. Barrett. 2024. "Mapping Rangeland Health Indicators in Eastern Africa from 2000 to 2022." *Earth System Science Data* 16 (11): 5375–5404. <https://doi.org/10.5194/essd-16-5375-2024>.
- The State Statistical Committee of the Republic of Azerbaijan 2023a. "Agriculture, Forestry and Fishing - Number of Animals and Poultry." Accessed February 23, 2023. <https://www.stat.gov.az/source/agriculture/>.
- Storch, T., H.-P. Honold, S. Chabrillat, M. Habermeyer, P. Tucker, M. Brell, A. Ohndorf, et al. 2023. "The enmap Imaging Spectroscopy Mission Towards Operations." *Remote Sensing of Environment* 294:113632. <https://doi.org/10.1016/j.rse.2023.113632>.
- Symeonakis, E. 2022. "Land Degradation Assessment with Earth Observation." *Remote Sensing* 14 (8): 1776. <https://doi.org/10.3390/rs14081776>.
- The State Statistical Committee of the Republic of Azerbaijan 2023b. "Agriculture, Forestry and Fishing - Population and Area." Accessed March 8, 2023. <https://www.stat.gov.az/source/agriculture/>.
- The State Statistical Committee of the Republic of Azerbaijan 2023c. "Agriculture, Forestry and Fishing - Utilised Agricultural Area." *The State Statistical Committee of the Republic of Azerbaijan*. Accessed March 8, 2023. <https://www.stat.gov.az/source/agriculture/>.
- Tsendbazar, N., L. Li, M. Koopman, S. Carter, M. Herold, I. Georgieva, and M. Lesiv. 2021. World Cover Product Validation Report (D12-PVR). https://esa-worldcover.s3.eu-central-1.amazonaws.com/v100/2020/docs/WorldCover_PVR_V1.1.pdf:esa.
- USGS. 2021. *Landsat 4-7 Collection 2 (C2) Level 2 Science Product (L2SP) Guide*. EROS, Sioux Falls, South Dakota: Department of the Interior, U.S. Geological Survey.
- USGS. 2022. *Landsat 8-9 Collection 2 (C2) Level 2 Science Product (L2SP) Guide*. EROS, Sioux Falls, South Dakota: Department of the Interior, U.S. Geological Survey.
- Vlek, P., Q. B. Le, and L. Tamene. 2010. "Assessment of Land Degradation, Its Possible Causes and Threat to Food Security in sub-Saharan Africa." In *Food Security and Soil Quality*, edited by R. Lal and B. A. Stewart, 57–86. Boca Raton: CRC Press.
- Wang, B., R. An, T. Jiang, F. Xing, and F. Ju. 2020. "Image Spectral Resolution Enhancement for Mapping Native Plant Species in a Typical Area of the three-River Headwaters Region, China." *Remote Sensing* 12 (19). <https://doi.org/10.3390/rs12193146>.
- Wessels, K. J., S. D. Prince, P. E. Frost, and D. van Zyl. 2004. "Assessing the Effects of Human-Induced Land Degradation in the Former Homelands of Northern South Africa with a 1 Km AVHRR NDVI Time-Series." *Remote Sensing of Environment* 91 (1): 47–67. <https://doi.org/10.1016/j.rse.2004.02.005>.
- White, M. A., G. P. Asner, R. R. Nemani, J. L. Privette, and S. W. Running. 2000. "Measuring Fractional Cover and Leaf Area Index in Arid Ecosystems: Digital Camera, Radiation Transmittance, and Laser Altimetry Methods." *Remote Sensing of Environment* 74 (1): 45–57. [https://doi.org/10.1016/S0034-4257\(00\)00119-X](https://doi.org/10.1016/S0034-4257(00)00119-X).
- Wiesmair, M., H. Feilhauer, A. Magiera, A. Otte, and R. Waldhardt. 2016. "Estimating Vegetation Cover from high-Resolution Satellite Data to Assess Grassland Degradation in the Georgian Caucasus." *Mountain Research and Development* 36 (1): 56–65. <https://doi.org/10.1659/MRD-JOURNAL-D-15-00064.1>.
- Wiesmair, M., A. Otte, and R. Waldhardt. 2017. "Relationships Between Plant Diversity, Vegetation Cover, and Site Conditions: Implications for Grassland Conservation in the Greater Caucasus." *Biodiversity and Conservation* 26 (2): 273–291. <https://doi.org/10.1007/s10531-016-1240-5>.
- Yue, Y., M. Li, A. Zhu, X. Ye, R. Mao, J. Wan, and J. Dong. 2016. "Land Degradation Monitoring in the Ordos Plateau of China Using an Expert Knowledge and bp-ANN-Based Approach." *Sustainability* 8 (11): 1174. <https://doi.org/10.3390/su8111174>.

- Zanaga, D., R. Van De Kerchove, W. De Keersmaecker, N. Souverijns, C. Brockmann, R. Quast, J. Wevers, et al. 2021. "ESA worldcover 10 M 2020 v100." In. <https://zenodo.org/records/5571936>.
- Zhang, X., C. Liao, J. Li, and Q. Sun. 2013. "Fractional Vegetation Cover Estimation in Arid and Semi-Arid Environments Using hj-1 Satellite Hyperspectral Data." *International Journal of Applied Earth Observation and Geoinformation* 21:506–512. <https://doi.org/10.1016/j.jag.2012.07.003>.
- Zhao, Y., C. Chang, X. Zhou, G. Zhang, and J. Wang. 2024. "Land Use Significantly Improved Grassland Degradation and Desertification States in China Over the Last Two Decades." *Journal of Environmental Management* 349:119419. <https://doi.org/10.1016/j.jenvman.2023.119419>.
- Zhongming, W., B. G. Lees, J. Feng, L. Wanning, and S. Haijing. 2010. "Stratified Vegetation Cover Index: A New Way to Assess Vegetation Impact on Soil Erosion." *Catena* 83 (1): 87–93. <https://doi.org/10.1016/j.catena.2010.07.006>.
- Zhu, Z., S. Wang, and C. E. Woodcock. 2015. "Improvement and Expansion of the Fmask Algorithm: Cloud, Cloud Shadow, and Snow Detection for Landsats 4–7, 8, and Sentinel 2 Images." *Remote Sensing of Environment* 159:269–277. <https://doi.org/10.1016/j.rse.2014.12.014>.
- Ziel, V., M. Bachmann, F. Paulik, D. Rogge, S. Holzwarth, and U. Heiden. 2019. "FRANCA—A Fully Automated, Hyperspectral Processing Chain for FRActional Cover Analysis." *11th EARSeL SIG-IS workshop*, Brno, Czech Republic.